Progressive myoclonus epilepsies-Residual unsolved cases have marked genetic heterogeneity including dolichol-dependent protein glycosylation pathway genes

Courage, Carolina

2021-04-01

Courage , C , Oliver , K L , Park , E J , Cameron , J M , Grabinska , K A , Muona , M , Canafoglia , L , Gambardella , A , Said , E , Afawi , Z , Baykan , B , Brandt , C , di Bonaventura , C , Chew , H B , Criscuolo , C , Dibbens , L M , Castellotti , B , Riguzzi , P , Labate , A , Filla , A , Giallonardo , A T , Berecki , G , Jackson , C B , Joensuu , T , Damiano , J A , Kivity , S , Korczyn , A , Palotie , A , Striano , P , Uccellini , D , Giuliano , L , Andermann , E , Scheffer , I E , Michelucci , R , Bahlo , M , Franceschetti , S , Sessa , W C , Berkovic , S F & Lehesjoki , A-E 2021 , ' Progressive myoclonus epilepsies-Residual unsolved cases have marked genetic heterogeneity including dolichol-dependent protein glycosylation pathway genes ' , American Journal of Human Genetics , vol. 108 , no. 4 , pp. 722-738 . https://doi.org/10.1016/j.ajhg.2021.03.013

http://hdl.handle.net/10138/338557
https://doi.org/10.1016/j.ajhg.2021.03.013

Progressive myoclonus epilepsies – residual unsolved cases have marked genetic heterogeneity including genes in the dolichol-dependent protein glycosylation pathway

Carolina Courage,[1,37] Karen L. Oliver,[2,3,4,37] Eon Joo Park,[5] Jillian M. Cameron,[2] Kariona A. Grabińska,[5] Mikko Muona,[6,7] Laura Canafoglia,[8] Antonio Gambardella,[9] Edith Said,[10,11] Zaid Afawi,[12] Betul Baykan,[13] Christian Brandt,[14] Carlo di Bonaventura,[15] Hui Bein Chew,[16] Chiara Criscuolo,[17] Leanne M. Dibbens,[18] Barbara Castellotti,[19] Patrizia Riguzzi,[20] Angelo Labate,[9] Alessandro Filla,[17] Anna T. Giallonardo,[21] Geza Berecki,[22] Christopher B. Jackson,[23] Tarja Joensuu,[1] John A. Damiano,[2] Sara Kivity,[24] Amos Korczyn,[25] Aarno Palotie,[26,27,28] Pasquale Striano,[29] Davide Uccellini,[30] Loretta Giuliano,[31] Eva Andermann,[32,33] Ingrid E. Scheffer,[2,34,35,36] Roberto Michelucci,[20] Melanie Bahlo,[3,4] Silvana Franceschetti,[8] William C. Sessa,[5] Samuel F. Berkovic,[2,38]* Anna-Elina Lehesjoki[1,38]**

[1] Folkhälsan Research Center, Helsinki, Finland; Department of Medical and Clinical Genetics, Medicum, University of Helsinki, Finland
[2] Epilepsy Research Centre, Department of Medicine, University of Melbourne, Austin Health, Heidelberg, Victoria, Australia.
[3] Population Health and Immunity Division, the Walter and Eliza Hall Institute of Medical Research, Parkville, 3052, VIC, Australia.
[4] Department of Medical Biology, the University of Melbourne, Melbourne, 3010, VIC, Australia.
[5] Department of Pharmacology and Vascular Biology and Therapeutics Program, Yale University School of Medicine, 10 Amistad Street, New Haven, CT 06520, USA.
[6] Folkhälsan Research Center, Helsinki, Finland.
[7] Blueprint Genetics, Helsinki, Finland
[8] Neurophysiopathology, Fondazione IRCCS Istituto Neurologico Carlo Besta, Milan, Italy.
[9] Institute of Neurology, University Magna Græcia, Catanzaro, Italy.
[10] Section of Medical Genetics, Mater dei Hospital, Msida, Malta.
[11] Department of Anatomy and Cell Biology, University of Malta, Msida, Malta.
[12] Center for Neuroscience, Ben-Gurion University of the Negev, Be'er Sheva, Israel.
[13] Departments of Neurology and Clinical Neurophysiology, Istanbul Faculty of Medicine, Istanbul University, Istanbul, Turkey.
[14] Epilepsy Center Bethel, Bielefeld, Germany.
[15] Department of Human Neurosciences, Sapienza University of Rome, Viale dell'Università, 30, 00185, Rome, Italy.
[16] Genetics Department, Kuala Lumpur Hospital, Ministry of Health Malaysia, Jalan Pahang, 50586, Kuala Lumpur, Malaysia
[17] Department of Neuroscience, Reproductive, and Odontostomatological Sciences, University of Naples Federico II, Naples, Italy.
[18] Epilepsy Research Group, Australian Centre for Precision Health, UniSA Clinical and Health Sciences, University of South Australia, Adelaide 5000, Australia.
[19] Unit of Genetics of Neurodegenerative and Metabolic Diseases, IRCCS Istituto Neurologico Carlo Besta Milan, Italy.
[20] IRCCS Istituto delle Scienze Neurologiche di Bologna, Unit of Neurology, Bellaria Hospital, Bologna, Italy.
[21] Neurology Unit, Human Neurosciences Department, Sapienza University, Rome, Italy.

[22] Ion Channels and Disease Group, Florey Institute of Neuroscience and Mental Health, University of Melbourne, Parkville, Victoria, Australia.
[23] Stem Cells and Metabolism Research Program, Faculty of Medicine, University of Helsinki, 00290 Helsinki, Finland.
[24] Epilepsy Unit, Schneider Children's Medical Center of Israel, Petah Tiqvah, Israel.
[25] Sackler Faculty of Medicine, Tel Aviv University, Tel Aviv, Israel.
[26] Institute for Molecular Medicine Finland (FIMM), HiLIFE, University of Helsinki, Helsinki, Finland.
[27] Analytic and Translational Genetics Unit, Department of Medicine, Department of Neurology and Department of Psychiatry Massachusetts General Hospital, Boston, MA, USA.
[28] The Stanley Center for Psychiatric Research and Program in Medical and Population Genetics, The Broad Institute of MIT and Harvard, Cambridge, Boston, MA, USA.
[29] Pediatric Neurology and Muscular Diseases Unit, IRCCS Istituto "G. Gaslini", Genova, Italy.
[30] Neurology - Neurophysiology Unit, ASST dei Sette Laghi, Galmarini Tradate Hospital, Tradate, Italy
[31] Dipartimento "G.F. Ingrassia", Università degli Studi di Catania, Catania, Italy.
[32] Neurogenetics Unit and Epilepsy Research Group, Montreal Neurological Hospital and Institute, Montreal, Quebec, Canada.
[33] Departments of Neurology & Neurosurgery and Human Genetics, McGill University, Montreal, Quebec, Canada.
[34] Murdoch Children's Research Institute, Royal Children's Hospital, Parkville, VIC, 3052, Australia.
[35] Department of Paediatrics, The University of Melbourne, Royal Children's Hospital, Parkville, VIC, 3052, Australia.
[36] The Florey Institute, Parkville, VIC, 3052, Australia.

[37,38] These authors contributed equally to this work

Corresponding authors:

*Prof Dr Sam Berkovic
245 Burgundy St
Heidelberg, VIC
Australia 3084
E-mail: s.berkovic@unimelb.edu.au

**Prof Dr Anna-Elina Lehesjoki
Haartmaninkatu 8
00290 Helsinki
Finland
E-mail: anna-elina.lehesjoki@helsinki.fi

Abbreviations:

cisPTase – cis-Prenyltransferase

CNV – Copy number variant

CPY – Carboxypeptidase Y

DEE – Developmental and epileptic encephalopathy

GnomAD – Genome aggregation database

PME – Progressive myoclonus epilepsy

ULD – Unverricht-Lundborg disease

WES – Whole-exome sequencing

Keywords: Progressive myoclonus epilepsy; dolichol-dependent glycosylation; whole exome sequencing

Abstract

Progressive myoclonus epilepsies (PMEs) comprise a group of clinically and genetically heterogeneous rare diseases. Over 70% of PME cases can now be molecularly solved. Known PME genes encode a variety of proteins, many involved in lysosomal and endosomal function. We performed whole-exome sequencing (WES) in 84 (78 unrelated) unsolved PME patients, with or without additional family members, to discover novel causes. We identified likely disease-causing variants in 24 out of 78 (31%) unrelated patients, despite previous genetic analyses. The diagnostic yield was significantly higher for cases studied as trios or families (14/28) versus singletons (10/50) (OR = 3.9, p-value = 0.01, Fisher's exact test). The 24 likely solved cases involved 18 genes. First, we found and functionally validated five heterozygous variants in *NUS1* and *DHDDS* and a homozygous variant in *ALG10,* with no previous disease associations. All three genes are involved in dolichol-dependent protein glycosylation, a pathway not previously implicated in PME. Second, we independently validate *SEMA6B* as a new dominant PME gene in two unrelated patients. Third, in five families, we identified variants in established PME genes; three with intronic or copy-number changes (*CLN6, GBA, NEU1*) and two very rare causes (*ASAH1*, *CERS1*). Fourth, we found a group of genes usually associated with developmental and epileptic encephalopathies, but here, remarkably, presenting as PME, with or without prior developmental delay. Our systematic analysis of these cases, suggests that the small residuum of unsolved cases will most likely be a collection of very rare, genetically heterogeneous etiologies.

Introduction

The progressive myoclonus epilepsies (PMEs) are a group of rare clinically and genetically heterogeneous disorders that typically present in childhood or adolescence with action myoclonus, generalized tonic-clonic seizures, and progressive neurological decline.[1] The majority of PMEs follow autosomal recessive inheritance, with rare mitochondrial causes and a small, but increasing number of autosomal dominant genes.[2,3]

Clinically, the PMEs can be categorized into two broad groups. In one group, cognition is largely preserved with clinical features dominated by severe, treatment-resistant and physically disabling myoclonus, tonic-clonic seizures and ataxia.[1] The most common and paradigmatic form is Unverricht-Lundborg disease (ULD, EPM1), which is caused by recessive mutation, most commonly a dodecamer repeat expansion, of cystatin B (*CSTB*). The second clinical group is associated with significant cognitive impairment and decline, with the major forms including Lafora disease (EPM2A/B) and the neuronal ceroid lipofuscinoses (NCLs) which involve a number of recessive genes.

Known PME genes encode a variety of proteins, many of which have an endosomal and lysosomal function (Table S1). Despite this, there is no apparent unifying pathway leading to the phenotype.[4,5] Importantly a molecular genetic diagnosis will currently be made with an established PME gene in approximately 70% of all patients diagnosed with PME.[2]

We previously performed a whole-exome sequencing (WES) study on a cohort of 84 molecularly unsolved and unrelated singleton cases of PME. We identified a recurrent pathogenic variant in *KCNC1* (p.Arg320His) as a new cause of PME now known as MEAK (Myoclonus epilepsy and ataxia due to K+ channel mutation, EPM7).[3,6] This heterozygous variant not only added a new autosomal dominant gene to the list of known PME genes, but also highlighted a role for *de novo* pathogenic variants in PME.

In this study, we aimed to identify further causative genes for the unsolved PMEs by expanding our WES data analysis to include new unsolved patients and using, where possible, a trio-design approach to enhance the detection of *de novo* pathogenic variants.

Subjects and Methods

Patients

We studied a total of 84 (78 unrelated) molecularly unsolved patients (45 males) who had been clinically diagnosed with PME. Patients were referred for genetic research from centers in Europe, Australia and the USA over 25 years. Informed consent for DNA analysis was obtained from patients in line with local institutional review board requirements at the time of collection.

The majority of the cohort had previously had extensive genetic investigations, including clinical microarray and gene panel analyses (including mitochondrial gene testing where suspected), or singleton WES as part of our earlier research (n=57).[3] Specifically, all patients had been screened and tested negative for recessive variants in *CSTB*, including the dodecamer repeat expansion, and for the *KCNC1* recurrent pathogenic p.Arg320His variant.

A trio-design approach was used for 22/78 unrelated cases (28%) where DNA was available for both unaffected parents for WES. Six unrelated patients were exome sequenced with an affected first-degree relative (parent-child, n=2; or sibling pairs, n=4); two of the four sibling pairs had both unaffected parents available for WES and were analyzed as a quartet. The remaining 50 patients were analyzed as WES singletons (Figure S1).

Exome sequencing

This study included two sequencing cohorts (Figure S1). The first cohort comprised 57 singleton patients with PME that remained unsolved after our initial study;[3] of these, 44 did not have parental DNA available for trio- or quartet- WES re-analysis. This cohort was exome sequenced previously at the Wellcome Sanger Institute, Cambridge, UK in 2011-2012 (details of sequencing described in Muona, et al. 2015).[3]

The second cohort comprised a total of 40 patients with PME and 48 unaffected parents (contributing to 22 trios and 2 quartets). 27 PME cases in cohort 2 were newly referred patients; 13 were cases from cohort 1 that were re-sequenced with their parents. Exome sequencing for this cohort was performed at the Broad Institute of MIT and Harvard, Cambridge, MA, USA in 2015-2016. In detail, genomic DNA (approximately 1 µg) extracted from peripheral blood for each sample was enzymatically sheared in whole-exome library preparation. In-solution hybrid exome capture was performed using the Illumina Rapid Capture Exome enrichment kit with 38Mb target region (29Mb baited), which includes 98.3% of the intervals in the RefSeq exome database. Sequencing was performed on either Illumina HiSeq 4000 or HiSeq X instrument with the use of 151bp paired-end reads. The mean average sequencing depth for each sample was 78-fold, with more than 80% of target bases having at least 30-fold coverage. Mitochondrial DNA (mtDNA) was not targeted in either sequencing cohort.

Variant calling

Sequence reads were processed as described previously.[3] Variant calling of single nucleotide variants and indels was done by GATK HaplotypeCaller using joint calling approach. Thirteen patients underwent WES twice, in the previous study and here, so their sequence data was merged to maximize coverage. Variant quality scores were recalibrated jointly with GATK VariantRecalibrator. A truth

sensitivity cutoff of 99.8% was used for both SNVs and indels. *De novo* variants were called by GATK GenotypeRefinement and GATK PossibleDeNovo tools.

Sex and pedigree checks

Sex and ancestry checks for all samples and relatedness checks between all sample pairs were estimated using Peddy.[7] Inbreeding coefficients for all samples were estimated using FEstim.[8]

Variant annotation

Variant consequences were annotated using Variant Effect Predictor tool.[9] *In silico* prediction of deleterious variants was carried out by CADD,[10] SIFT,[11] PolyPhen2[12] and, in the case of splicing variants, Transcript inferred Pathogenicity (TraP) Score.[13] Variant allele frequencies were obtained primarily from the Genome Aggregation Database (gnomADv2.1.1). Gene-phenotype associations were annotated based on OMIM database and Clinical Genomics Database.

Variant filtering

To identify potentially pathogenic variants from the annotated data, all variants within 8 bp of exonic regions were filtered based on the potential modes of inheritance: X-linked, autosomal recessive, dominant and *de novo* using a similar approach to previously.[3] In recessive filtering, the exome data were analyzed for rare (<150 heterozygous counts and no homozygotes in the gnomADv2.1.1 database)[14] homozygous or compound heterozygous variants including missense, nonsense, splice site, inframe insertion and deletion and frameshift variants based on Variant Effect Predictor annotations in CCDS genes (Ensembl release 88). In the dominant filtering strategy (applied to both singleton cases, affected parent-child pairs and the *de novo* variant analysis), we included heterozygous variants with <5 counts in gnomADv2.1.1.

Variant prioritisation

Variants surviving the filtering steps were manually assessed and prioritized. All prioritised variants were classified according to ACMG standards and guidelines.[15] As these guidelines are not designed for novel research findings, and because they do not always capture the phenotypic subtleties, we also used a study-specific method of classification. We combined three lines of evidence: 1) at the variant level (e.g., using *in silico* prediction tools), 2) at the pedigree level (e.g., variant segregation data within families), and 3) at the gene level (e.g., prior disease phenotype associations). Each variant was given a score between 0-2 for the three lines of evidence making the maximum score 6 (Table S2).

We deemed variants as causative with "high confidence" if a score ≥ 5 was achieved; "moderate confidence" for variants with scores ≥ 4. Variants scoring < 4 were not prioritized or reported without the support of functional data.

Variant validation and segregation

Candidate variants in known and potentially novel disease genes were confirmed by bi-directional Sanger sequencing (ABI BigDye 3.1, Applied Biosystems) on ABI3730xl DNA Analyser. Primers were designed with Primer-BLAST.[16] The sequences were analysed using Sequencher v.5.3 (Gene Codes Corporation).

Specific splicing *in silico* predictions were made using Human Splicing Finder v3.1. Confirmation of *CLN6* splicing effect was performed by RT-PCR from total RNA extracted from patient fibroblast cells followed by sequencing of the abnormal amplicon (Figure S4).

Deletion confirmation of *NEU1* was performed by quantitative PCR (qPCR) (Figure S5).

Primers for Sanger sequencing and PCR are available upon request.

Copy number variant analysis from WES data

Copy number variants were called from the WES data based on relative sequencing depth. CNVkit was used to call the variants.[17] This analysis was performed separately for WES data generated in the original study[3] and in the current one owing to the different exome capture kits used. CNV analysis focused on known disease genes (annotated against Clinical Genomics Database), in particular those associated with PMEs.

Analysis of short tandem repeats

We additionally examined whether any of the probands had short tandem repeats (STRs) that were expanded at 27 known pathogenic loci (Table S3). The WES samples were examined separately using two STR detection tools, Expansion Hunter v.2.5.5[18] and exSTRa.[19] For each locus we looked for evidence of outlying samples in terms of STR length by inspecting plots of estimated STR size (ExpansionHunter), and empirical cumulative distribution function (eCDF; exSTRa) plots of the number of repeated bases observed for each sample.

Human fibroblast culture

Fibroblast cultures were established from skin biopsy samples of patients PME1, PME2, PME71 and PME27 as well as controls. Cells were cultured in DMEM (Gibco, Thermo Scientific) plus 10% FBS, 100 units/mL penicillin, 100 µg/mL streptomycin, and 2mM glutamine in a 37 °C and 5% CO_2 humidified incubator.

Microsomal cis-prenyltransferase activity measurement

Crude microsomes were prepared as described[20] with minor modifications. Cis-prenyltransferase (cisPTase) assays and activity measurements in human dermal fibroblasts were performed as described[21,22] with minor modifications. In brief, microsomal fractions from cells were prepared by centrifugation at 100 000 g for 40 min at 4°C. 50 µg microsomal protein was used for cisPTase activity measurement with reaction mixture containing 45 µM FPP, 50 µM [1- 14C]- isopentenyl

pyrophosphate (IPP) (55 mCi/mmol), 25 mM Tris–HCl, pH 7.4, 5 mM $MgCl_2$, 1.25 mM DTT, 2.5 mM sodium orthovanadate, 10 μM Zaragozic acid A and 0.35% Triton X-100. Reactions were performed at 37°C for 1 hr and stopped by the addition 4 ml of chloroform:methanol (3:2 ratio). The protein pellet was removed by centrifugation and the supernatant was washed three times with 1/5 volume of 10 mM EDTA in 0.9% NaCl. The incorporation of radioactive IPP into organic fraction containing polyprenyl pyrophosphate was measured by scintillation counting.

Western blot analysis

Cells were washed twice with ice-cold PBS and lysed in lysis buffer (50 mM Tris-HCl, 1% NP-40, 0.1% SDS, 0.1% Deoxycholic Acid, 0.1 mM EDTA, 0.1 mM EGTA, protease and phosphatase inhibitors). Protein extracts were separated by SDS-PAGE and then transferred to nitrocellulose membrane. Primary antibodies against NUS1 (Abcam, ab168351), DHDDS (Sigma, HPA026727), ICAM1 (Santa Cruz, Sc8439), LAMP1 (BD Transduction Laboratories, 611402), and HSP90 (Cell Signaling Technology, 4877) were used. The appropriate LI-COR secondary IRDye antibodies and LI-COR Odyssey Infrared Imaging System (LI-COR, Lincoln, NE) were used for antibody detection.

Filipin staining

Cells were grown on glass cover glasses, fixed in 4% PFA for 10 min and permeablized in 0.1% TritonX-100 for 5 min. Cells were then incubated with 50 μg/ml filipin (Sigma, F4767) for 1 hr. As a positive control for induction of cholesterol accumulation, cells were treated for 16 hr with 1 μM U18666A (EMD Biosciences). Relative intensity of filipin staining was quantified by calculating average pixel intensity using Adobe Photoshop according to the equation: average filipin intensity = total intensity above low threshold/number of pixels above low threshold.[23]

Yeast strains and culture methods

S. cerevisiae strain *alg10*Δ (MATa his3Δ1 leu2Δ0 met15Δ0 ura3Δ0 YGR227W::kanX4, Dharmacon) and its derivatives were used. Cultures were grown at 30°C in YPD or Synthetic minimal medium made of 0.67% (wt/vol) yeast nitrogen base and 2% (wt/vol) glucose supplemented with auxotrophic requirements. For solid media, agar (Becton Dickinson) was added at a 2% (wt/vol) final concentration. Yeast transformations were performed by standard yeast genetic methods.

Functional characterization of ALG10/ALG10B variants in yeast

To examine the functionality of hALG10 proteins, the N-glycosylation status of carboxypeptidase Y (CPY) was tested in *S. cerevisiae alg10*Δ strain transformed with empty pKG-GW1 plasmid (2μ, LEU2 marker[21]) (negative control) or pKG-GW1 carrying yeast (y) ALG10 ORF (positive control), human (h) ALG10, hALG10 p.Lys391Valfs*35, hALG10B or hALG10B p.Leu253Trp. Yeast transformants were inoculated from single colony and grown overnight at 30°C in synthetic medium lacking leucine. Cells from saturated overnight cultures were harvested and lysed by alkaline method. Whole-cell lysate (WCL) was subjected to SDS PAGE (7.5% gel) and immunoblotting. Yeast CPY was detected with anti-CPY monoclonal antibodies (Fisher Scientific, clone 10A5B5).

Statistical and data analysis

Statistical analyses and graphical representation were performed with the GraphPad Prism v.7.0 software (GraphPad Software, inc., USA) or the R statistical programming language (version number 3.6.1.). Figure legends indicate the statistical test used in functional experiments. P-values <0.05 were considered significant.

Gene co-expression networks

For gene co-expression analyses, normalised brain expression values from the BrainSpan Developmental transcriptome dataset were downloaded from http://www.brainspan.org. Genes were

removed if they had expression values missing from >50% of the 524 samples available from 42 individuals.

Using the log2 transformed expression values, a matrix of weighted correlations was generated, with weights determined as $1/\sqrt{n}$, where n is the number of samples contributed by the respective individual. Correlation plots were visualized using the corrplot R package, with genes ordered by hierarchical clustering, using the median linkage method.

To determine whether the established and candidate PME genes were more highly co-expressed than expected by chance we randomly sampled 5,000 sets of genes. We calculated the median $|\rho|$ for each random gene set and compared this to the observed median $|\rho|$ of the PME gene set.

Results

Patient cohort

The study cohort included 84 patients with PME from 78 families who did not have a known molecular basis. Genomic ancestry checks suggested 74 families (95%) were of European descent, with more than half (n=46) referred from hospital centres in Italy. The other four families were admixed American (n=2) and East Asian (n=2). Inbreeding estimates using FEstim suggested 24% of families were consanguineous (19/78). This was consistent with clinical descriptions of parental relatedness in ten families; detailed pedigree histories were not available for the other nine.

Clinically, the majority of the 78 unrelated patients were classified into the two well-established groups: 43% (n=34) had "ULD-like" (i.e. classical childhood/adolescent onset of PME; no dementia) and 31% (n=24) as PME + dementia. Two smaller groups comprised developmental delay predating PME onset (n=12) and a group of late-onset (>20 years) PME cases (n=8) (Figure 1). Age of disease onset across the cohort ranged from late infancy to 45 years (mean 12 years) (Figure S2).

In total, we identified variants in 24 out of 78 (31%) unrelated patients that we regarded with moderate-to-high confidence (see Methods) as causative. Interestingly, the diagnostic success was highest in one of the two newly recognised, rarer clinical groups (PME with prior developmental delay), although the numbers were small (Figure 1).

We had the most success with cases in whom we had sequenced additional family members (14/28); we identified a likely causal variant in 45% of trios and in 67% of cases where another affected 1st-degree relative was sequenced. The proportion of singletons with likely causative variants was significantly less, with just 10 out of 50 cases (OR = 3.9, p-value = 0.01, Fisher's exact test).

The 24 likely solved cases involved 18 genes; one (*ALG10*) has no known disease associations, 6 were known PME genes, including the very recently described *SEMA6B*, and 11 have been reported in other neurological diseases, but not previously in PME (Figure 2, Tables 1-3, S4-S5).

Dolichol-dependent glycosylation identified as a novel PME pathway

In discovering variants in *NUS1*, *DHDDS* and *ALG10* in a total of 6 unrelated subjects, we identified dolichol-dependent glycosylation as a novel disease pathway for PME (Figure 2 and Figure S3). The age of onset and clinical features were heterogeneous (Table 1).

We subsequently functionally characterized the variants in these three related genes. *NUS1* and *DHDDS* encode two subunits of cisPTase (also known as dehydrodolichyl diphosphate synthase), the first enzyme committed to dolichol synthesis (Figure S3D).[21,22,24,25] CisPTase is located at a critical branchpoint of farnesyl diphosphate metabolism, with an alternate branch responsible for cholesterol synthesis. *ALG10* is more distal in the dolichol pathway; it is a glucosyltransferase that transfers the terminal glucose residue from dolichyl phosphate glucose (Dol-P-Glc) onto the lipid-linked oligosaccharide precursor Glc2Man9GlcNAc(2)-PP-Dol. The terminal glucose residue added is a key element required for efficient N-linked glycosylation of proteins.[26]

NUS1

Two patients had variants in *NUS1* (NM_138459.3; MIM: 610463; also termed NgBR), encoding the accessory subunit of cisPTase. Patient PME1 carried a *de novo* frameshift variant c.740dupT, p.Asp248Glyfs*15 and patient PME2 a *de novo* nonsense variant c.310delG, p.Val104* (Tables 1, S4, S5, Figure S2A).

Initial analysis of fibroblast cells by western blotting revealed decreased amount of NUS1 in patient cells compared to controls, implying the presence of nonsense mediated mRNA decay and/or instability of the truncated proteins (Figure 3B). In patient PME1, also the amount of DHDDS

appeared to be decreased, in line with the predicted truncated NUS1 product that is missing the interface region for heterodimerization with DHDDS and consequently DHDDS instability.[22,27,28] CisPTase activity in patient cells was drastically decreased, demonstrating that lower protein levels directly affect enzymatic turnover rates (Figure 3A). In order to evaluate the consequence of the reduced cisPTase activity in the patients' cells, the glycosylation status of ICAM1 and LAMP1, established markers for N-glycosylation defects,[29,30] was examined. Altered ICAM1 and LAMP1 expression and migration were detected by western blot analysis (Figure 3B). Finally, we examined free cholesterol levels, an additional consequence of NUS1 dysfunction in cells.[31] The patient fibroblasts were stained with filipin and free cholesterol pools were examined. Both patient fibroblasts exhibited increased accumulation of free cholesterol compared to controls (Figure 3C).

DHDDS

Three patients were identified with rare missense variants in *DHDDS* (NM_024887.3; MIM: 608172; also termed hCIT), encoding the catalytic subunit of cisPTase. Patient PME3 was found to have a *de novo* missense variant c.632G>A (p.Arg211Gln) previously described in three patients with DEE.[32,33] PME71 and PME27, carried heterozygous missense variants c.614G>A (p.Arg205Gln) and c.283G>A (p.Asp95Asn), respectively. No parental samples were available for PME71 for segregation analysis (Tables 1, S4, S5, Figure S2B). For PME27, it was only possible to exclude the c.283G>A variant in the father as maternal DNA was unavailable. PME27 was also heterozygous for a rare variant in *DNMT1* (c.1619A>G, p.(Tyr540Cys)), but without functional support this variant did not meet our criteria for prioritization (Table S6).

Functional studies in fibroblasts from patients PME71 and PME27 showed apparently normal amounts of both DHDDS and NUS1 (Figure 3B) in line with the preserved capacity for heterodimerization, decreased cisPTase activity in isolated membranes (Figure 3A) and altered levels and migration of ICAM1 and LAMP1 proteins indicating protein N-glycosylation defect (Figure 3B).

Furthermore, consistent with reduced cisPTase activity and protein glycosylation defect, increased cholesterol accumulation was detected in both fibroblast cells (Figure 3C). Fibroblasts were not available from PME3 but, because the variant was *de novo* and previously reported, we regarded it as disease causing with high confidence.

ALG10

Patient PME50 was included in the first exome study and identified to carry the homozygous frameshift variant c.1170_1171delAA (p.Lys391Valfs*35) (Tables 1, S4, S5, Figure S3C) in *ALG10* (NM_032834.3; MIM: 618355),[3] encoding a putative alpha-1,2-glucosyltransferase. At that time, with no prior disease association for *ALG10* and with no functional studies performed, the variant was regarded as of uncertain significance. Here, we now provide evidence for its pathogenicity.

Hypo-glycosylation of reporter proteins ICAM1 and LAMP1, identified in western blot analysis of patient fibroblasts (Figure 4A) predicts a defect in alpha-1,2-glucosyltransferase activity. To confirm the predicted function of ALG10 as an alpha-1,2-glucosyltransferase and to model the *ALG10* variant, we used a yeast alg10 deletion strain to re-express human wild-type and mutant ALG10 proteins for functional complementation. In the absence of dolichyl-phosphoglucose-dependent alpha-1,2-glucosyltransferase activity, the lipid-linked oligosaccharide (N-glycan precursor) lacking terminal glucose is less efficiently transferred to glycoprotein,[26] resulting in the reporter protein for N-glycosylation, CPY, being hypo-glycosylated and running more quickly on SDS-polyacrylamide gel electrophoresis. Both yeast and human ALG10 did complement the yeast deletion strain (Figure 4B), as judged by the presence of mainly the mature form of CPY. Alg10 deletion strains transformed either with empty vector or with mutated ALG10 (Figure 4B) showed multiple bands of CPY corresponding to hypo-glycosylated forms of the protein, thus supporting the pathogenicity of the *ALG10* p.Lys391Valfs*35 variant. Given that the *ALG10* variant was only detected in one patient and

has no established disease association, we classified it as disease causing with moderate confidence, despite the functional evidence for its pathogenicity.

The patient is, however, also homozygous for a missense variant c.758T>G, p.(Leu253Trp) in the highly homologous *ALG10B* gene encoding alpha-1,2-glucosyltransferase B (NM_001013620; MIM 603313).[34] The missense variant is reported in gnomAD with an allele frequency of 0.004 with 5 homozygous individuals so it is unlikely to be pathogenic on its own. However, whilst human ALG10B complemented glycosylation in the yeast assay, the variant ALG10B was not quite as effective (Figure 4B), so we could not rule out a contribution of the homozygous *ALG10B* variant to the phenotype.

Likely causative variants in established PME genes

In seven families, we identified likely causative variants in established PME genes (*SEMA6B, CLN6, GBA, NEU1, CERS1, ASAH1*) (Table 2). These cases all defied diagnosis earlier because of unusual genetic mechanisms or very rare or newly recognized causes.

SEMA6B (MIM: 608873) was recently published as a new dominant PME gene with *de novo* variants in 4 cases.[35] We independently validate this finding with an additional two cases (PME83, PME25). Both of our cases had frameshift variants in the last exon of *SEMA6B* (Table 2) within very close proximity to the published series.[35] Low coverage, due to high GC content, of this exon meant that only one of the two variants were initially called by our bioinformatics pipeline and thus both variants escaped detection until targeted *SEMA6B* reanalysis (Figure S3). Clinically, PME83 and PME25 were classified as PME with developmental delay, consistent with the published cases (Table S5). We confirmed the *de novo* status for PME83 by subsequent Sanger sequencing of the parents, but parental DNA was unavailable for PME25.

In the case of the *CLN6* (MIM: 6067259) and *GBA* (MIM: 606463) genes, the putative causative variants (Table 2) are both intronic and were not prioritised by initial filtering strategies. Prior to genetic testing, the patients were clinically suspected of having Kufs Type A and Gaucher disease respectively.[36,37] Both variants are homozygous and inbreeding coefficient estimates were consistent with parental consanguinity for the two families. Predictions for the *GBA* splice-site variant having an effect on mRNA splicing was consistent across all splicing *in silico* tools, however, without the ability to confirm this experimentally (patient deceased) we classified the variant as likely causative with moderate confidence. The deep intronic *CLN6* variant was predicted *in silico* to create an intronic exonic splicing enhancer (ESE) site[38] and RT-PCR from patient-derived fibroblast cells confirmed aberrant mRNA splicing (Figure S4A). Sanger sequencing of the aberrant product revealed inclusion of 119 nucleotides of intronic sequence downstream from the 3' end of exon 4 (Figure S4B). These data are compatible with the homozygous variant in the patient causing activation of a non-canonical splice site through creation of an intronic ESE site (Figure S4C). The intronic inclusion creates a premature stop codon after 60 nucleotides of open reading frame in the intronic sequence. This is predicted to result in nonsense-mediated decay with partial loss of functional protein, compatible with the late onset CLN6 disease in the patient. As such we classified this variant as likely causative with high confidence (Figure 2; Tables S4, S5).

Our single CNV finding was at the *NEU1* (MIM: 608272) locus. In this patient, WES data initially suggested a homozygous c.544A>G, p.(Ser182Gly) *NEU1* variant (Table 2). Validation by Sanger sequencing showed that only the mother was a heterozygous carrier of the missense variant. Reanalysis of the WES data for a potential CNV in the region indicated the presence of a deletion on the paternal allele, confirmed by quantitative PCR (Figure S5). Subsequently, the patient's younger brother developed symptoms and genetic analysis confirmed his compound heterozygous status for the same *NEU1* variants. Clinically the presentation for both brothers was consistent with sialidosis,[39]

although thorough eye examinations were normal; no cherry-red spot was seen in either (Tables S4 and S5).

Recessive variants in very rare PME genes involved in the sphingolipid pathway, *CERS1*[40] (MIM: 606919) and *ASAH1*,[41] (MIM: 613468) were identified in one family each. Siblings PME7 and PME8 were homozygous for two variants in *CERS1*, a nonsense and a missense variant (Table 2). Segregation analysis confirmed heterozygosity for both variants in one of the parents respectively. The parents were known to be related, with consistent inbreeding F estimates. In patient PME9, WES revealed compound heterozygous variants in *ASAH1*, one splice-site and one missense variant (Tables 2, S4 and S5); at diagnosis the patient had PME but not spinal muscular atrophy although this subsequently developed.

Likely causative variants in other known disease genes

An additional 11 likely causative variants were identified in genes not previously associated with PME, but recognized in neurological phenotypes including seizures or ataxia (Table 3). *CHD2* (MIM: 602119), *CACNA2D2* (MIM: 607082) and *CACNA1A* (MIM: 601011) are established DEE genes, as are *NUS1* and *DHDDS* involved in dolichol metabolism (see above). *CACNA1A* is also associated with ataxia syndromes as are *STUB1* (MIM: 607207) and *CAMTA1* (MIM: 611501).

PEX19 (MIM: 600279), *NAXE* (MIM: 608862), *RARS2* (MIM: 611524) and *DYNC1H1* (MIM: 600112) are currently associated with more complex neurological phenotypes (Table 3). These variants all met our criteria for moderate to high confidence in causation based on both the genetic data and phenotypic overlap (Tables S4 and S5) (see Methods).

In the case of *PEX19*, this is a well-established gene for peroxisome biogenesis disorders. We identified three patients (PME21, PME22, PME60), from two unrelated families of Maltese origin, with the same homozygous missense variant c.254C>T, p.(Ala85Val). All three patients shared a similar phenotype with onset around age 9 years involving myoclonus, tonic-clonic seizures, ataxia,

cognitive decline and marked photosensitivity (Tables 3 and S5). Patient PME60 had a clinically similarly affected brother who was deceased and not tested. This variant is not present in the Maltese Genome project[42] with 400 individuals; however, haplotype analysis results were consistent with a distant founder effect (Figure S6). Further, independent studies have identified two additional Maltese patients with the same homozygous variant and similar clinical phenotype (data not shown).

Filtered variants that did not meet our criteria for prioritisation can be found in Table S6. Our short tandem repeat analyses did not detect any expansions at the known pathogenic loci (Table S3).

PME gene brain co-expression networks

Using brain expression data from *BrainSpan*, we examined the co-expression between the major established PME genes (Table S1) and all genes we report here with likely causative variants (Tables 1, 2 and 3). Expression data was not available for *MT-TK* responsible for myoclonus epilepsy associated with ragged-red fibers (MERRF); this mitochondrial gene was therefore excluded from the analysis.

The ordered correlation matrices revealed some striking patterns (Figure 5). We observed 3 large clusters of eleven positively correlated gene sets that accounted for all candidate and established (**bold**) PME genes. Cluster one contains: ***NHLRC1***, ***CLN3***, ***ATN1***, *DHDDS*, *CACNA2D2*, ***KCNC1***, *CACNA1A*, *CAMTA1*, ***DNAJC5***, *DYNC1H1*, ***HTT***. Cluster two contains: ***CLN6***, ***CLN8***, ***EPM2A***, ***TPP1***, ***GBA***, ***NEU1***, *PEX19*, *STUB1*, *NAXE*, ***SEMA6B***, ***CERS1***. Cluster three contains: ***CSTB***, ***CLN5***, ***ASAH1***, ***MFSD8***, *NUS1*, ***GOSR2***, ***SCARB2***, *ALG10*, ***KCTD7***, *RARS2*, *CHD2*.

Using a Monte Carlo sampling approach, we found evidence that the established and candidate PME genes were more highly co-expressed than would be expected by chance ($p < 0.05$). These results suggest that overall these genes have similar brain gene expression signatures. Shared biological networks are further supported by the observation that clusters 2 and 3 are negatively correlated.

Discussion

Our data uncovered dolichol-dependent protein glycosylation as a new pathway underlying PME. Additional important findings were the confirmation of *SEMA6B* as a new cause of PME and that PME can sometimes be a rare manifestation of variants in genes associated with developmental and epileptic encephalopathy or ataxia syndromes. Finally, our results suggest that there is unlikely to be a major shared genetic basis to the remaining unsolved cases, but rather the answer will most likely be a heterogenous mix of rare disorders. However, rare variants in a novel gene, particularly in the introns, and regions of low coverage cannot be excluded.

Overall, we identified plausible pathogenic variants in 24 out of 78 (31%) unrelated cases. This cohort of patients had been extensively studied for known genetic causes previously, so, it is notable that our diagnostic yield was this high. As *de novo* dominant mutations were recently established as an important alternative cause of PME,[3] we pursued a trio-design WES analysis where possible. Overall, we had significantly greater success identifying plausible pathogenic variants in cases that had been sequenced with other family members (i.e. as an affected trio- or quartet- with unaffected parents or part of an affected sibling or parent-offspring pair). This was driven in part by the importance of *de novo* variants in dominant genes (n=5), that has previously been under-appreciated for this disease group, but also the ability to confirm compound heterozygosity and/or homozygosity for variants (n=9) under a recessive model. Clinically, the two primary categories of PME have historically been separated according to the presence (PME with dementia) or absence ("ULD-like") of cognitive decline. In this analysis of cases defying molecular diagnosis, two additional clinical groups were apparent; PME with prior developmental delay and a late-onset group. Our success rate in diagnosis was highest for one of the newly recognised, albeit smaller, clinical groups: 50% for PME patients with prior developmental delay (Figure 1).

We associate a novel biological pathway, dolichol-dependent glycosylation, with the PME phenotype through the identification of variants in *NUS1*, *DHDDS* and *ALG10* supported by demonstrating glycosylation defects in patient-derived fibroblast cell lines and/or in yeast assays. Protein glycosylation is a ubiquitous post-translational modification that contributes to several crucial biological and physiological processes within cells. Given that variants in *NUS1*, *DHDDS* and *ALG10* were associated with altered expression and migration of ICAM1 and LAMP1, and since ALG10 is specifically linked to N-glycosylation, it is plausible that variants in these genes result in N-glycosylation defects in cells. [22,27-30] N-glycosylation followed by oligomannose phosphorylation of the N-glycated protein is pivotal for lysosomal targeting of enzymes.[43] Given that defects in many lysosomal enzymes have been associated with PME, hypoglycosylation caused by impaired N-glycosylation of such proteins may be contributing to the phenotype in patients with mutations in *NUS1*, *DHDDS* and *ALG10*. However, the exact mechanisms would need to be explored in further functional studies. Of note, dolichol metabolism was first associated with PME over 30 years ago with the observation that dolichol content was significantly increased in the brains and urinary sediment of NCL patients.[44,45] The reason for this observation remained unknown but was postulated to be caused by a possible defect in dolichol recycling or metabolism. PME now joins the expanding list of phenotypes included under the rubric of congenital disorders of glycosylation, which are quite clinically heterogeneous.[46] Unlike most of the established PME genes where the clinical presentation is somewhat characteristic for each gene, the clinical picture of the dolichol pathway genes (Table 1) is more reminiscent of *TBC1D24* where the clinical spectrum is much wider.[47]

A handful of pathogenic variants in *NUS1* and *DHDDS* have previously been associated with various phenotypes. Biallelic mutations in both genes have been reported in single families with congenital disorders of glycosylation showing severe, multiorgan manifestations,[21,48] and in *DHDDS* additionally with retinitis pigmentosa.[49] More recently, heterozygous *de novo* variants in both *NUS1* and *DHDDS* were reported in DEE patients.[32,33] Interestingly, one of these *DHDDS* variants was

identified in one of the PME patients in our cohort. *NUS1* variants have also been associated with early-onset Parkinson disease with an increase in rare variant burden in PD cases versus controls.[50] Remarkably, variants in two established recessive PME genes, *GBA* and *SCARB2*, are also risk alleles for Parkinson disease.[51-53] Finally, the recent *NUS1* reports of a recurrent heterozygous *de novo* variant in two unrelated patients with epilepsy, myoclonus and ataxia[54] and an autosomal dominant family with epilepsy, ataxia and tremor segregating a heterozygous frameshift variant,[55] support our conclusion that *NUS1* is a new PME gene. However, it is clear that the phenotypic spectrum for both *NUS1* and *DHDDS* is broad.

The majority of proteins involved in the N-glycosylation pathway (like *NUS1* and *DHDDS*) have been associated with mainly autosomal recessive congenital disorders of glycosylation.[56] *ALG10* is a rare exception as it has previously not been associated with any clinical phenotype, the only exception being our report of it as a candidate gene for PME based on the identification of a homozygous frameshift variant in one patient.[3] Here, through functional characterization of this variant, we give further support for *ALG10* being a novel PME gene. However, despite functional evidence implying pathogenicity of the reported *ALG10* variant, further patients should be identified to establish *ALG10* as a disease gene. Interestingly, the patient was also homozygous for a missense variant in the highly homologous *ALG10B* gene (also known as *KCR1*),[34] that has not been previously associated with any human recessive disorder. Our yeast complementation data imply that the *ALG10B* variant may be a hypomorph with attenuated ability for transferring the glucose residue to the lipid-linked oligosaccharide precursor. In the absence of ALG10 activity, this may not be enough to maintain a proper level of cellular transferase activity. It is therefore possible that compromised function of both genes is required for an *ALG10*-related disease to manifest.

Patients with PME are typically cognitively normal prior to epilepsy onset. Here we highlight a rare group with prior developmental delay (n=12); six with plausible genetic findings. Importantly, two

of the six had heterozygous frameshift variants in *SEMA6B*. *SEMA6B* was recently discovered as a rare PME gene, with frameshift variants all occurring in the GC-rich last exon of this gene[35] in 4 subjects. They had mild initial developmental delay, seizure onset between 11 months and 6 years with subsequent cognitive and motor regression, needing assistance with ambulation by the early second decade. Microcephaly and spasticity were present in some. All were regarded as having severe intellectual disability and they were all alive at ages 12-28 years. Our cases had a similar course (Table S5), but did not have microcephaly or significant spasticity and the level of intellectual disability was moderate-severe. To date they have survived until 38 and 39 years without further deterioration, unlike the pattern seen in some PMEs due to storage disorders and those with mutations in *SCARB2* or *GOSR2* with prominent early adult deterioration and often early death.

Traditionally, PME and DEE are regarded as distinct syndromic groups; this distinction continues to be practically useful. However, it is now clear that the boundary between these groups is blurred, both from a genetic and phenotypic view point. The other four developmentally delayed PME patients with molecular findings had variants in established DEE genes. This included (confirmed or presumed) *de novo* variants in *DHDDS* (n=2) and *CHD2*; and a fourth case due to recessive *CACNA2D2* mutation. Here, we associate these three DEE genes with PME for the first time, building on our initial study where we expanded the *TBC1D24* phenotypic spectrum to PME.[3] Similarly, *KCNA2*, another established DEE gene, was recently reported in a single PME case.[57] In the reverse direction, after we discovered *KCNC1* as a causative *de novo* dominant PME gene, it has now also been established as an important DEE gene, although the causative mutations differ.[58]

We also report putative pathogenic variants in a handful of known ataxia genes (Table 3), both recessive and dominant. These genes join *ARG3L2* and *SACS* reported in our initial study[3] as known ataxia genes with pathogenic variants in patients with PME. We had a small number of patients in our cohort of 84 patients who had no reported tonic-clonic seizures making their clinical presentation

more consistent with progressive myoclonic ataxia (PMA). This clinical overlap, with both PME and PMA presentations, is well-established for genes such as *GOSR2* and *KCNC1*.[6,59] We also identified interesting variants in other known neurological disease genes (Table 3) that not only significantly broaden the genetic basis to the PMEs, but also highlight the need for further functional studies and larger patient numbers to fully understand genotype-phenotype correlations.

The brain gene co-expression analysis uncovered some potentially important relationships between established PME and newly reported PME genes. The advantage of using a brain-specific resource for this analysis, such as *BrainSpan*, is the detection of brain-specific signatures. An additional advantage of the brain gene co-expression approach is that it is not biased against genes with little known about their function or limited by published material as can be the case for other network generating data sources (e.g., protein-protein interactions or text-mining). The observation that three PME genes associated with the sphingolipid pathway (i.e., *CERS1*, *NEU1*, *GBA*) cluster together in gene set 2 (Figure 5) is proof of principle for the unbiased gene co-expression approach. As such, the clustering of genes that have not previously been biologically associated may indeed be highlighting novel biological pathways.

Future perspective

The PMEs are the genetically best-characterized group of epilepsies. They are highly genetically heterogeneous and there are founder effects, resulting in a different distribution of particular types of PME in various populations. The most comprehensive study of ~200 cases from Italy reached a diagnosis in ~70% of cases although not all were fully investigated.[2] A number of the residual cases have been diagnosed subsequently, including via this study. Future whole-genome sequencing approaches such as long read sequencing, as well as improved bioinformatic software (e.g. for structural variant calling, repeat expansion detection) likely hold the key to uncovering the elusive genetic basis to these remaining rare genetic disorders.

We only report one pathogenic CNV in this study, but we cannot rule out CNVs as a more important genetic factor due again to exome sequencing data being limited in its ability to detect such genetic variants. The same argument is true for the detection of repeat expansions. Over half of the known disease-causing repeat expansions are located in intronic and UTR gene regions that are not well captured by exome sequencing data, thus it is not perhaps surprising we had no positive results from this analysis. The recent discovery of pathogenic intronic pentanucleotide expansions in Familial Adult Myoclonic Epilepsy (FAME), a dominant disorder that is on the mild end of severity of the PME spectrum, reinforces the relevance and importance of searching for known and novel repeat expansions in genetically unsolved PME patients.[60-63]

Our experience with this cohort has highlighted just how genetically heterogeneous the residuum of unsolved patients with PME are. Of the remaining unsolved cases, they are unlikely to include another gene affecting a large proportion of cases like *KCNC1*,[3] but rather a collection of multiple rare genetic causes. Collectively, we estimate that it is now less than 20% of PME patients that cannot be attributed to known disease-genes with intronic variants possibly going undetected in previous analyses as was the case for our *CLN6* and *GBA* positive cases. The detection and interpretation of such variants will only improve as the field transitions from exome sequencing to whole-genome sequencing.

Supplemental Data

Supplemental Data include 7 figures and 6 tables

Data and Code Availability

WES data have not been deposited in a public repository due to privacy and ethical restrictions.

Declaration of Interests

Mikko Muona is employed by Blueprint Genetics. All other authors declare no competing interests.

Acknowledgements

The authors are indebted to the families participating in this study. We thank Paula Hakala, Katri Aksentjeff, Saara Tegelberg, Simona Allievi and Marta Bayly for technical support, and Michael Hildebrand for molecular analysis.

Following funding bodies are acknowledged: Swiss National Foundation (Early Postdoc Mobility Grant [to C.C.]), Folkhälsan Research Foundation [to A.-E.L.], NIH grant R35 HL139945 [to W.C.S.], Australian National Health and Medical Research Council (NHMRC) Program Grants (GNT1054618) [to M.B.] (GNT1091593) [to S.F.B. and I.E.S.], NHMRC Senior Research Fellowship (GNT1102971) and Independent Research Institute Infrastructure Support Scheme (IRIISS) [to M.B.], Victorian Government's Operational Infrastructure Support Program [to M.B.], Istanbul University Scientific Research Fund-BAP-2019K12-149071 [to B.B.], NHMRC Senior Research Fellowship (GNT1104718) [to L.M.D.]; NHMRC Practitioner Fellowship (GNT1104831) [to I.E.S.]. A.-E.L. is a HiLIFE Fellow at the University of Helsinki.

Web Resources

BrainSpan, http://www.brainspan.org

GnomAD v2.1.1, http://gnomad.broadinstitute.org

Human Splicing Finder v3.1, http://umd.be/Redirect.html

OMIM, http://www.omim.org

TraP, http://trap-score.org

References

1. Berkovic, S.F., Andermann, F., Carpenter, S., and Wolfe, L.S. (1986). Progressive myoclonus epilepsies: specific causes and diagnosis. N Engl J Med 315, 296-305.
2. Franceschetti, S., Michelucci, R., Canafoglia, L., Striano, P., Gambardella, A., Magaudda, A., Tinuper, P., La Neve, A., Ferlazzo, E., Gobbi, G., et al. (2014). Progressive myoclonic epilepsies: definitive and still undetermined causes. Neurology 82, 405-411.
3. Muona, M., Berkovic, S.F., Dibbens, L.M., Oliver, K.L., Maljevic, S., Bayly, M.A., Joensuu, T., Canafoglia, L., Franceschetti, S., Michelucci, R., et al. (2015). A recurrent de novo mutation in KCNC1 causes progressive myoclonus epilepsy. Nat Genet 47, 39-46.
4. Ramachandran, N., Girard, J.M., Turnbull, J., and Minassian, B.A. (2009). The autosomal recessively inherited progressive myoclonus epilepsies and their genes. Epilepsia 50 Suppl 5, 29-36.
5. Kollmann, K., Uusi-Rauva, K., Scifo, E., Tyynela, J., Jalanko, A., and Braulke, T. (2013). Cell biology and function of neuronal ceroid lipofuscinosis-related proteins. Biochim Biophys Acta 1832, 1866-1881.
6. Oliver, K.L., Franceschetti, S., Milligan, C.J., Muona, M., Mandelstam, S.A., Canafoglia, L., Boguszewska-Chachulska, A.M., Korczyn, A.D., Bisulli, F., Di Bonaventura, C., et al. (2017). Myoclonus epilepsy and ataxia due to KCNC1 mutation: Analysis of 20 cases and K(+) channel properties. Ann Neurol 81, 677-689.
7. Pedersen, B.S., and Quinlan, A.R. (2017). Who's Who? Detecting and Resolving Sample Anomalies in Human DNA Sequencing Studies with Peddy. Am J Hum Genet 100, 406-413.
8. Leutenegger, A.L., Labalme, A., Genin, E., Toutain, A., Steichen, E., Clerget-Darpoux, F., and Edery, P. (2006). Using genomic inbreeding coefficient estimates for homozygosity mapping of rare recessive traits: application to Taybi-Linder syndrome. Am J Hum Genet 79, 62-66.
9. McLaren, W., Gil, L., Hunt, S.E., Riat, H.S., Ritchie, G.R., Thormann, A., Flicek, P., and Cunningham, F. (2016). The Ensembl Variant Effect Predictor. Genome Biol 17, 122.
10. Rentzsch, P., Witten, D., Cooper, G.M., Shendure, J., and Kircher, M. (2019). CADD: predicting the deleteriousness of variants throughout the human genome. Nucleic Acids Res 47, D886-D894.
11. Sim, N.L., Kumar, P., Hu, J., Henikoff, S., Schneider, G., and Ng, P.C. (2012). SIFT web server: predicting effects of amino acid substitutions on proteins. Nucleic Acids Res 40, W452-457.
12. Adzhubei, I.A., Schmidt, S., Peshkin, L., Ramensky, V.E., Gerasimova, A., Bork, P., Kondrashov, A.S., and Sunyaev, S.R. (2010). A method and server for predicting damaging missense mutations. Nat Methods 7, 248-249.
13. Gelfman, S., Wang, Q., McSweeney, K.M., Ren, Z., La Carpia, F., Halvorsen, M., Schoch, K., Ratzon, F., Heinzen, E.L., Boland, M.J., et al. (2017). Annotating pathogenic non-coding variants in genic regions. Nat Commun 8, 236.
14. Karczewski, K.J., Francioli, L.C., Tiao, G., Cummings, B.B., Alföldi, J., Wang, Q., Collins, R.L., Laricchia, K.M., Ganna, A., Birnbaum, D.P., et al. (2020). The mutational constraint spectrum quantified from variation in 141,456 humans. Nature 581, 434-443.
15. Richards, S., Aziz, N., Bale, S., Bick, D., Das, S., Gastier-Foster, J., Grody, W.W., Hegde, M., Lyon, E., Spector, E., et al. (2015). Standards and guidelines for the interpretation of sequence variants: a joint consensus recommendation of the American College of Medical Genetics and Genomics and the Association for Molecular Pathology. Genet Med 17, 405-424.
16. Ye, J., Coulouris, G., Zaretskaya, I., Cutcutache, I., Rozen, S., and Madden, T.L. (2012). Primer-BLAST: a tool to design target-specific primers for polymerase chain reaction. BMC Bioinformatics 13, 134.
17. Talevich, E., Shain, A.H., Botton, T., and Bastian, B.C. (2016). CNVkit: Genome-Wide Copy Number Detection and Visualization from Targeted DNA Sequencing. PLoS Comput Biol 12, e1004873.
18. Dolzhenko, E., van Vugt, J., Shaw, R.J., Bekritsky, M.A., van Blitterswijk, M., Narzisi, G., Ajay, S.S., Rajan, V., Lajoie, B.R., Johnson, N.H., et al. (2017). Detection of long repeat expansions from PCR-free whole-genome sequence data. Genome Res 27, 1895-1903.
19. Tankard, R.M., Bennett, M.F., Degorski, P., Delatycki, M.B., Lockhart, P.J., and Bahlo, M. (2018). Detecting Expansions of Tandem Repeats in Cohorts Sequenced with Short-Read Sequencing Data. Am J Hum Genet 103, 858-873.
20. Rush, J.S., Matveev, S., Guan, Z., Raetz, C.R., and Waechter, C.J. (2010). Expression of functional bacterial undecaprenyl pyrophosphate synthase in the yeast rer2{Delta} mutant and CHO cells. Glycobiology 20, 1585-1593.
21. Park, E.J., Grabinska, K.A., Guan, Z., Stranecky, V., Hartmannova, H., Hodanova, K., Baresova, V., Sovova, J., Jozsef, L., Ondruskova, N., et al. (2014). Mutation of Nogo-B receptor, a subunit of cis-prenyltransferase, causes a congenital disorder of glycosylation. Cell Metab 20, 448-457.
22. Harrison, K.D., Park, E.J., Gao, N., Kuo, A., Rush, J.S., Waechter, C.J., Lehrman, M.A., and Sessa, W.C. (2011). Nogo-B receptor is necessary for cellular dolichol biosynthesis and protein N-glycosylation. EMBO J 30, 2490-2500.

23. Pipalia, N.H., Huang, A., Ralph, H., Rujoi, M., and Maxfield, F.R. (2006). Automated microscopy screening for compounds that partially revert cholesterol accumulation in Niemann-Pick C cells. J Lipid Res 47, 284-301.
24. Grabińska, K.A., Edani, B.H., Park, E.J., Kraehling, J.R., and Sessa, W.C. (2017). A conserved C-terminal RXG motif in the NgBR subunit of cis-prenyltransferase is critical for prenyltransferase activity. Journal of Biological Chemistry 292, 17351-17361.
25. Grabinska, K.A., Park, E.J., and Sessa, W.C. (2016). cis-Prenyltransferase: New Insights into Protein Glycosylation, Rubber Synthesis, and Human Diseases. J Biol Chem 291, 18582-18590.
26. Burda, P., and Aebi, M. (1998). The ALG10 locus of Saccharomyces cerevisiae encodes the α-1, 2 glucosyltransferase of the endoplasmic reticulum: the terminal glucose of the lipid-linked oligosaccharide is required for efficient N-linked glycosylation. Glycobiology 8, 455-462.
27. Edani, B.H., Grabinska, K.A., Zhang, R., Park, E.J., Siciliano, B., Surmacz, L., Ha, Y., and Sessa, W.C. (2020). Structural elucidation of the cis-prenyltransferase NgBR/DHDDS complex reveals insights in regulation of protein glycosylation. Proc Natl Acad Sci U S A 117, 20794-20802.
28. Bar-El, M.L., Vankova, P., Yeheskel, A., Simhaev, L., Engel, H., Man, P., Haitin, Y., and Giladi, M. (2020). Structural basis of heterotetrameric assembly and disease mutations in the human cis-prenyltransferase complex. Nat Commun 11, 5273.
29. Medina-Cano, D., Ucuncu, E., Nguyen, L.S., Nicouleau, M., Lipecka, J., Bizot, J.C., Thiel, C., Foulquier, F., Lefort, N., Faivre-Sarrailh, C., et al. (2018). High N-glycan multiplicity is critical for neuronal adhesion and sensitizes the developing cerebellum to N-glycosylation defect. Elife 7.
30. He, P., Ng, B.G., Losfeld, M.E., Zhu, W., and Freeze, H.H. (2012). Identification of intercellular cell adhesion molecule 1 (ICAM-1) as a hypoglycosylation marker in congenital disorders of glycosylation cells. J Biol Chem 287, 18210-18217.
31. Harrison, K.D., Miao, R.Q., Fernandez-Hernando, C., Suarez, Y., Davalos, A., and Sessa, W.C. (2009). Nogo-B receptor stabilizes Niemann-Pick type C2 protein and regulates intracellular cholesterol trafficking. Cell Metab 10, 208-218.
32. Hamdan, F.F., Myers, C.T., Cossette, P., Lemay, P., Spiegelman, D., Laporte, A.D., Nassif, C., Diallo, O., Monlong, J., Cadieux-Dion, M., et al. (2017). High Rate of Recurrent De Novo Mutations in Developmental and Epileptic Encephalopathies. Am J Hum Genet 101, 664-685.
33. Lelieveld, S.H., Reijnders, M.R., Pfundt, R., Yntema, H.G., Kamsteeg, E.J., de Vries, P., de Vries, B.B., Willemsen, M.H., Kleefstra, T., Lohner, K., et al. (2016). Meta-analysis of 2,104 trios provides support for 10 new genes for intellectual disability. Nat Neurosci 19, 1194-1196.
34. Nakajima, T., Hayashi, K., Viswanathan, P.C., Kim, M.-Y., Anghelescu, M., Barksdale, K.A., Shuai, W., Balser, J.R., and Kupershmidt, S. (2007). HERG is protected from pharmacological block by α-1, 2-glucosyltransferase function. Journal of Biological Chemistry 282, 5506-5513.
35. Hamanaka, K., Imagawa, E., Koshimizu, E., Miyatake, S., Tohyama, J., Yamagata, T., Miyauchi, A., Ekhilevitch, N., Nakamura, F., Kawashima, T., et al. (2020). De Novo Truncating Variants in the Last Exon of SEMA6B Cause Progressive Myoclonic Epilepsy. Am J Hum Genet 106, 549-558.
36. Arsov, T., Smith, K.R., Damiano, J., Franceschetti, S., Canafoglia, L., Bromhead, C.J., Andermann, E., Vears, D.F., Cossette, P., Rajagopalan, S., et al. (2011). Kufs disease, the major adult form of neuronal ceroid lipofuscinosis, caused by mutations in CLN6. Am J Hum Genet 88, 566-573.
37. Park, J.K., Orvisky, E., Tayebi, N., Kaneski, C., Lamarca, M.E., Stubblefield, B.K., Martin, B.M., Schiffmann, R., and Sidransky, E. (2003). Myoclonic epilepsy in Gaucher disease: genotype-phenotype insights from a rare patient subgroup. Pediatr Res 53, 387-395.
38. Vaz-Drago, R., Custodio, N., and Carmo-Fonseca, M. (2017). Deep intronic mutations and human disease. Hum Genet 136, 1093-1111.
39. Canafoglia, L., Robbiano, A., Pareyson, D., Panzica, F., Nanetti, L., Giovagnoli, A.R., Venerando, A., Gellera, C., Franceschetti, S., and Zara, F. (2014). Expanding sialidosis spectrum by genome-wide screening: NEU1 mutations in adult-onset myoclonus. Neurology 82, 2003-2006.
40. Vanni, N., Fruscione, F., Ferlazzo, E., Striano, P., Robbiano, A., Traverso, M., Sander, T., Falace, A., Gazzerro, E., Bramanti, P., et al. (2014). Impairment of ceramide synthesis causes a novel progressive myoclonus epilepsy. Ann Neurol 76, 206-212.
41. Zhou, J., Tawk, M., Tiziano, F.D., Veillet, J., Bayes, M., Nolent, F., Garcia, V., Servidei, S., Bertini, E., Castro-Giner, F., et al. (2012). Spinal muscular atrophy associated with progressive myoclonic epilepsy is caused by mutations in ASAH1. Am J Hum Genet 91, 5-14.
42. Vella, J., Fiott, A., Mizzi, C., Borg, J., Bugeja, M., Galdies, R., Cassar, W., Scerri, J., Scerri, C., and Felice, A. (2013). The Malta BioBank and the Maltese Genome Project.
43. Kim, J.-J.P., Olson, L.J., and Dahms, N.M. (2009). Carbohydrate recognition by the mannose-6-phosphate receptors. Current opinion in structural biology 19, 534-542.
44. Wolfe, L.S., Ng Ying Kin, N.M., Palo, J., and Haltia, M. (1983). Dolichols in brain and urinary sediment in neuronal ceroid lipofuscinosis. Neurology 33, 103-106.
45. Wolfe, L.S., Palo, J., Santavuori, P., Andermann, F., Andermann, E., Jacob, J.C., and Kolodny, E. (1986). Urinary sediment dolichols in the diagnosis of neuronal ceroid-lipofuscinosis. Ann Neurol 19, 270-274.
46. Sparks, S.E., and Krasnewich, D.M. (1993). Congenital Disorders of N-Linked Glycosylation and Multiple Pathway Overview. In GeneReviews((R)), M.P. Adam, H.H. Ardinger, R.A. Pagon, S.E. Wallace, L.J.H. Bean, K. Stephens, andA. Amemiya, eds. (Seattle (WA).
47. Balestrini, S., Milh, M., Castiglioni, C., Luthy, K., Finelli, M.J., Verstreken, P., Cardon, A., Strazisar, B.G., Holder, J.L., Jr., Lesca, G., et al. (2016). TBC1D24 genotype-phenotype correlation: Epilepsies and other neurologic features. Neurology 87, 77-85.
48. Sabry, S., Vuillaumier-Barrot, S., Mintet, E., Fasseu, M., Valayannopoulos, V., Heron, D., Dorison, N., Mignot, C., Seta, N., Chantret, I., et al. (2016). A case of fatal Type I congenital disorders of glycosylation (CDG I) associated with low dehydrodolichol diphosphate synthase (DHDDS) activity. Orphanet J Rare Dis 11, 84.
49. Zuchner, S., Dallman, J., Wen, R., Beecham, G., Naj, A., Farooq, A., Kohli, M.A., Whitehead, P.L., Hulme, W., Konidari, I., et al. (2011). Whole-exome sequencing links a variant in DHDDS to retinitis pigmentosa. Am J Hum Genet 88, 201-206.
50. Guo, J.F., Zhang, L., Li, K., Mei, J.P., Xue, J., Chen, J., Tang, X., Shen, L., Jiang, H., Chen, C., et al. (2018). Coding mutations in NUS1 contribute to Parkinson's disease. Proc Natl Acad Sci U S A 115, 11567-11572.
51. Gan-Or, Z., Dion, P.A., and Rouleau, G.A. (2015). Genetic perspective on the role of the autophagy-lysosome pathway in Parkinson disease. Autophagy 11, 1443-1457.
52. Michelakakis, H., Xiromerisiou, G., Dardiotis, E., Bozi, M., Vassilatis, D., Kountra, P.M., Patramani, G., Moraitou, M., Papadimitriou, D., Stamboulis, E., et al. (2012). Evidence of an association between the scavenger receptor class B member 2 gene and Parkinson's disease. Mov Disord 27, 400-405.

53. Aharon-Peretz, J., Rosenbaum, H., and Gershoni-Baruch, R. (2004). Mutations in the glucocerebrosidase gene and Parkinson's disease in Ashkenazi Jews. N Engl J Med 351, 1972-1977.
54. Den, K., Kudo, Y., Kato, M., Watanabe, K., Doi, H., Tanaka, F., Oguni, H., Miyatake, S., Mizuguchi, T., Takata, A., et al. (2019). Recurrent NUS1 canonical splice donor site mutation in two unrelated individuals with epilepsy, myoclonus, ataxia and scoliosis - a case report. BMC Neurol 19, 253.
55. Araki K, N.R., Ito D, Kato K, Iguchi Y, Sahashi K, Toyama, and M, H.K., Okamoto N, Wada Y, Nakamura T, Ogi T, Katsuno M. (2020). *NUS1* mutation in a family with epilepsy, cerebellar ataxia, and tremor. Epilepsy Research.
56. Ng, B.G., and Freeze, H.H. (2018). Perspectives on glycosylation and its congenital disorders. Trends in Genetics 34, 466-476.
57. Canafoglia, L., Castellotti, B., Ragona, F., Freri, E., Granata, T., Chiapparini, L., Gellera, C., Scaioli, V., Franceschetti, S., and DiFrancesco, J.C. (2019). Progressive myoclonus epilepsy caused by a gain-of-function KCNA2 mutation. Seizure 65, 106-108.
58. Cameron, J.M., Maljevic, S., Nair, U., Aung, Y.H., Cogne, B., Bezieau, S., Blair, E., Isidor, B., Zweier, C., Reis, A., et al. (2019). Encephalopathies with KCNC1 variants: genotype-phenotype-functional correlations. Ann Clin Transl Neurol 6, 1263-1272.
59. Boisse Lomax, L., Bayly, M.A., Hjalgrim, H., Moller, R.S., Vlaar, A.M., Aaberg, K.M., Marquardt, I., Gandolfo, L.C., Willemsen, M., Kamsteeg, E.J., et al. (2013). 'North Sea' progressive myoclonus epilepsy: phenotype of subjects with GOSR2 mutation. Brain 136, 1146-1154.
60. Ishiura, H., Doi, K., Mitsui, J., Yoshimura, J., Matsukawa, M.K., Fujiyama, A., Toyoshima, Y., Kakita, A., Takahashi, H., Suzuki, Y., et al. (2018). Expansions of intronic TTTCA and TTTTA repeats in benign adult familial myoclonic epilepsy. Nat Genet 50, 581-590.
61. Corbett, M.A., Kroes, T., Veneziano, L., Bennett, M.F., Florian, R., Schneider, A.L., Coppola, A., Licchetta, L., Franceschetti, S., Suppa, A., et al. (2019). Intronic ATTTC repeat expansions in STARD7 in familial adult myoclonic epilepsy linked to chromosome 2. Nat Commun 10, 4920.
62. Florian, R.T., Kraft, F., Leitao, E., Kaya, S., Klebe, S., Magnin, E., van Rootselaar, A.F., Buratti, J., Kuhnel, T., Schroder, C., et al. (2019). Unstable TTTTA/TTTCA expansions in MARCH6 are associated with Familial Adult Myoclonic Epilepsy type 3. Nat Commun 10, 4919.
63. Yeetong, P., Pongpanich, M., Srichomthong, C., Assawapitaksakul, A., Shotelersuk, V., Tantirukdham, N., Chunharas, C., Suphapeetiporn, K., and Shotelersuk, V. (2019). TTTCA repeat insertions in an intron of YEATS2 in benign adult familial myoclonic epilepsy type 4. Brain 142, 3360-3366.

Figure legends and Tables

Figure 1. Proportion of all 78 unrelated patients with (solved) and without (unsolved) likely pathogenic variants by clinical group.

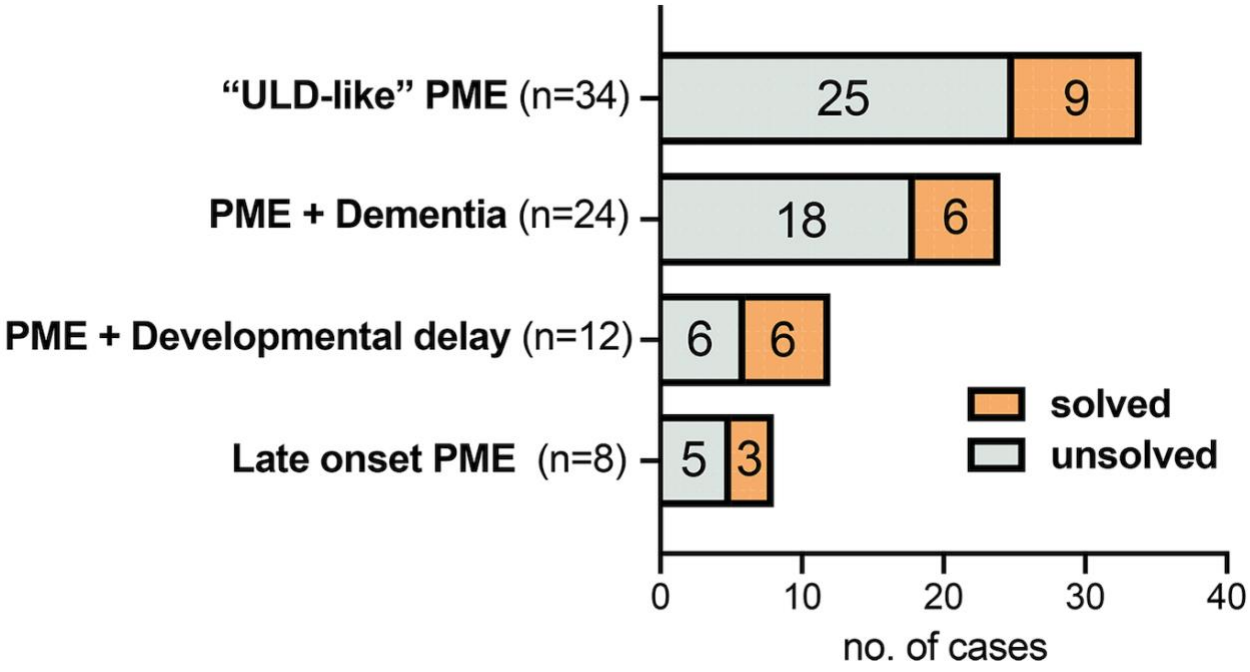

Figure 2. Novel and previously described PME-associated genes (n=18) with high and moderate confidence variants detected in our cohort of 78 unrelated patients that had previous extensive genetic investigations. The number of unrelated patients with variants in each gene is shown in parentheses with the known primary function/pathway of each gene also listed. See Methods for criteria followed when classifying variants as high versus moderate confidence. *Functionally validated genes in this study.

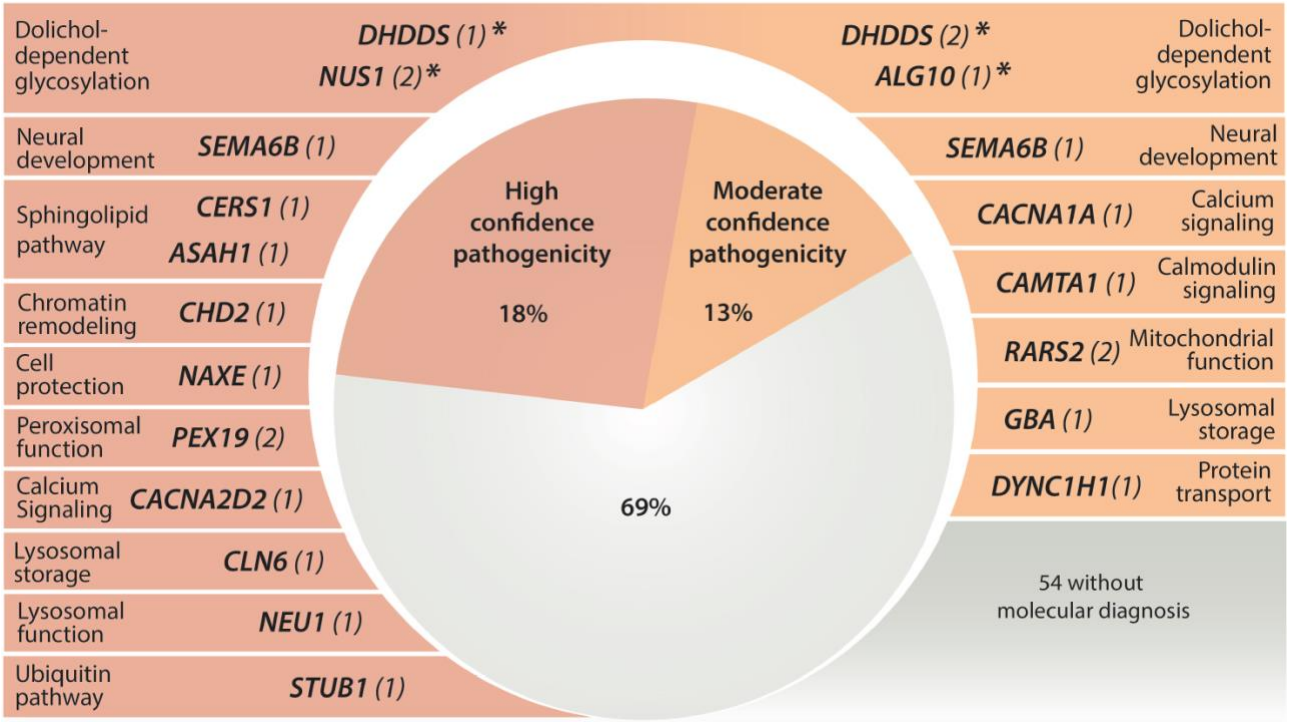

Figure 3. The *NUS1* and *DHDDS* variants cause defects in protein glycosylation due to reduced cisPTase activity in patient-derived fibroblast cell lines. (**A**) Reduced microsomal cisPTase activity in isolated membranes from patient (*NUS1*: PME1, PME2 and *DHDDS*: PME71, PME27) compared to control (C) fibroblasts. **p <0.005, ***p <0.001. (**B**) Affected protein glycosylation in patient fibroblasts. Western blot analysis of NUS1, DHDDS, LAMP1 and ICAM1 levels. HSP90 was used as loading control. (**C**) Increased cholesterol accumulation in patient fibroblasts. Filipin staining and quantitative representation from patient and control cells. U18666A was used as a positive control for inhibition of cholesterol trafficking. *p <0.05, **p <0.005, ***p <0.001, a.u., arbitrary units. Data are representative of at least 3 experiments.

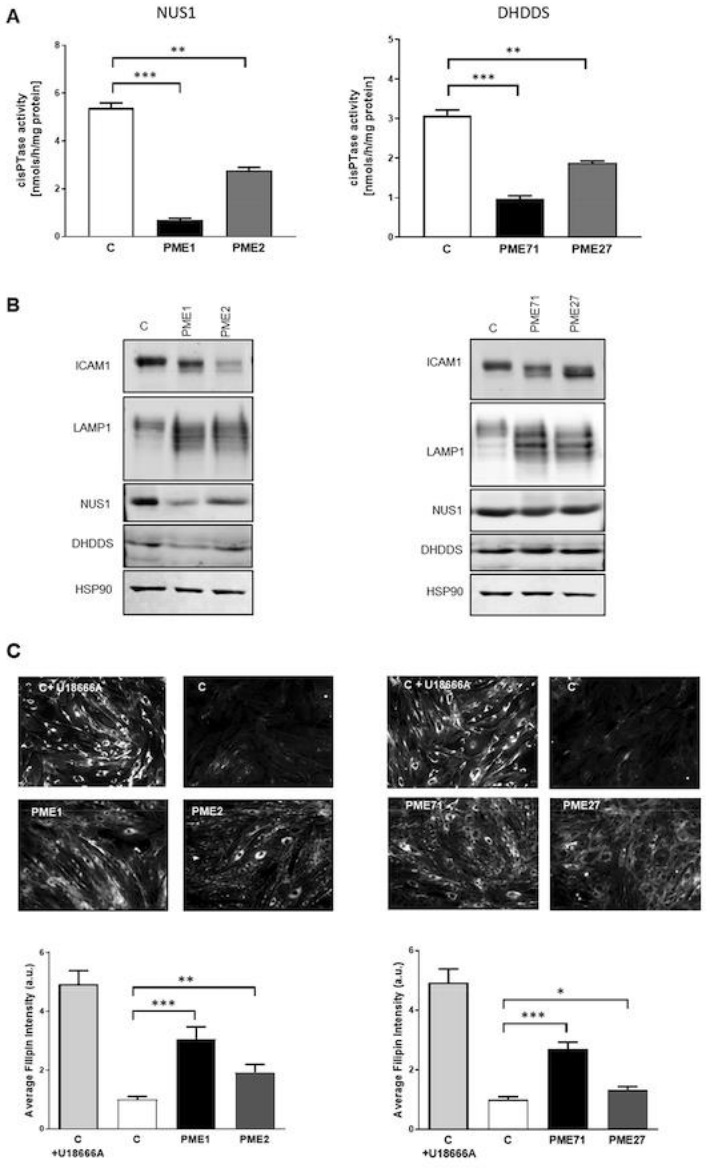

Figure 4. The *ALG10* frameshift mutation causes defects in protein N-glycosylation due to a predicted defect in alpha-1,2-glucosyltransferase activity. (A) Affected protein glycosylation in fibroblasts carrying the *ALG10* and *ALG10B* variants. Western blot analysis of ICAM1 and LAMP1 expression. HSP90 was used as loading control. **(B)** Protein N-glycosylation of CPY shows multiple hypo-glycosylated bands in a yeast alg10 deletion strain transformed with mutated human (h) ALG10 (hALG10fs) or empty vector. N-glycosylation deficiency is rescued when transformed with either wild-type yeast ALG10 (yALG10), hALG10 or hALG10B.

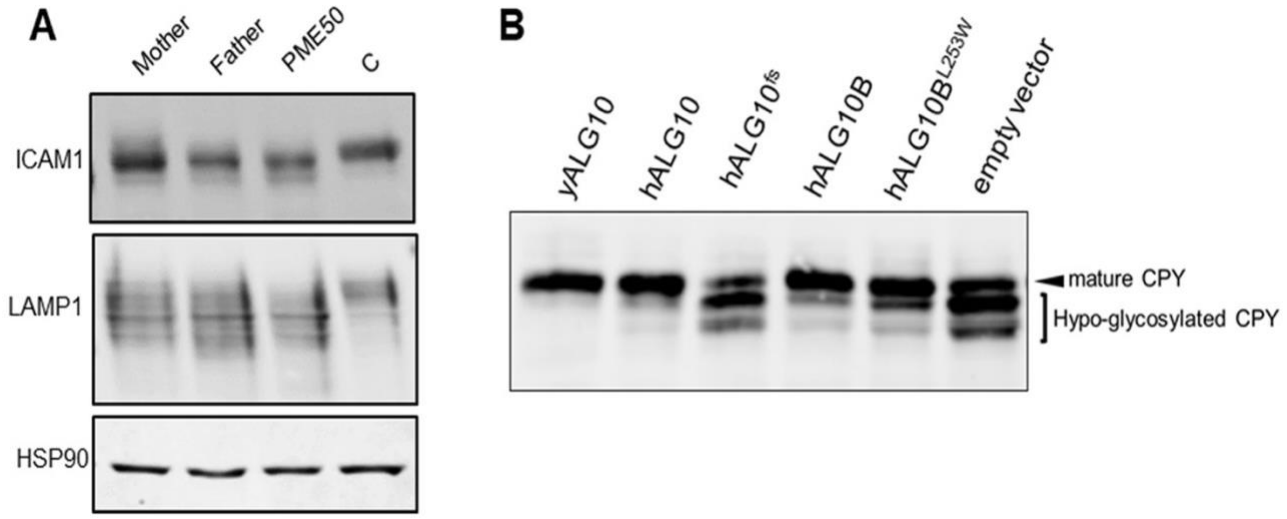

Figure 5. Gene co-expression matrix for 33 known (black) and candidate (grey) PME genes. Pairwise Spearman correlations between genes shown, based on 524 samples from 42 individuals from the BrainSpan resource. Genes are ordered and grouped with hierarchical clustering, using the median linkage method.

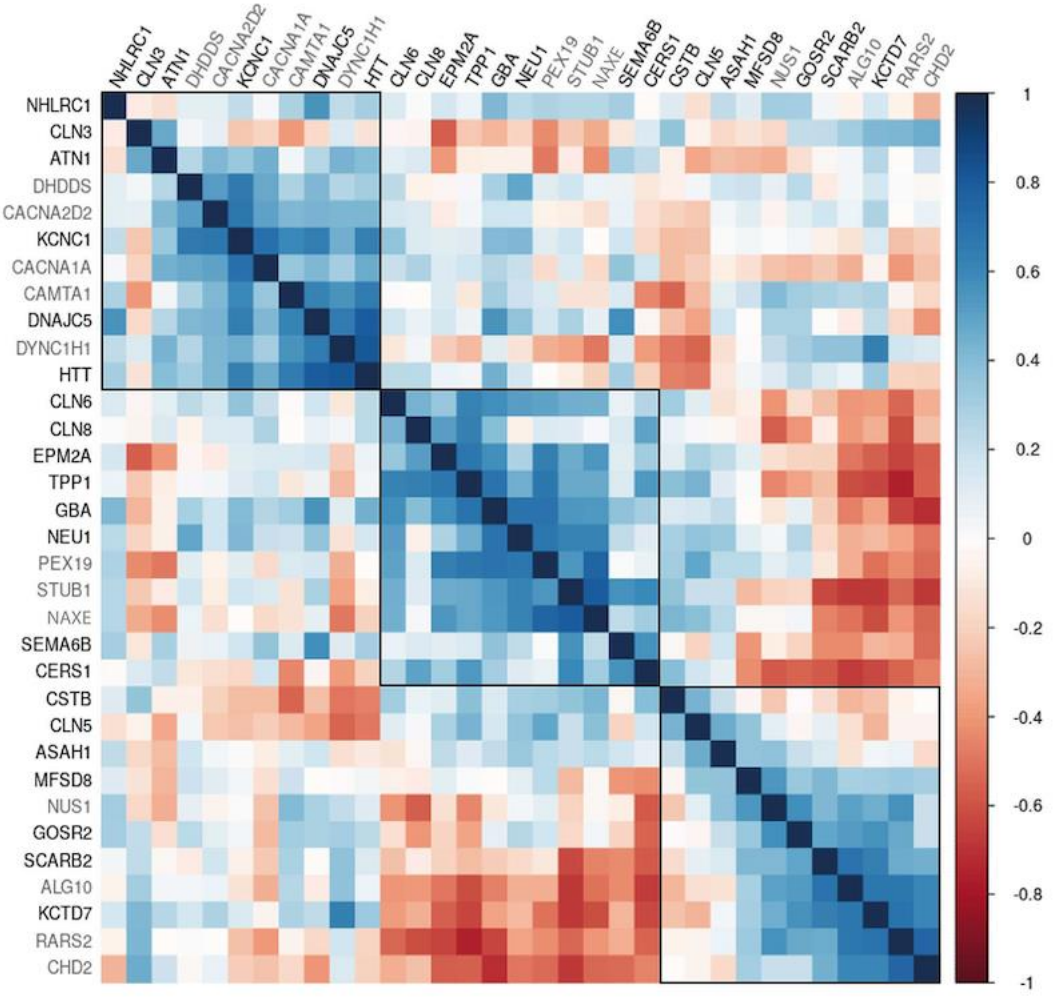

Table 1. Dolichol-dependent glycosylation genes with variants identified in this patient cohort

Patient ID Country of Origin	Sex	Gene	Variant(s)	gnomAD MAF	Inheritance	Clinical summary (onset age)	WES study design	Confidence
PME1 Italy	M	***NUS1***	c.740dupT; p.Asp248Glyfs*15 (het)	0	*de novo*	Myoclonus (13y), no seizures. No ataxia, normal cognition.	trio	high
PME2 Italy	F	***NUS1***	c.310delG; p.Val104* (het)	0	*de novo*	Absence with eyelid myoclonia (4y), myoclonus (8y), ataxia, moderate cognitive impairment. Febrile seizures (4y) with developmental regression.	trio	high
PME3 Italy	M	***DHDDS***	c.632G>A; p.Arg211Gln (het)	0	*de novo*	Myoclonus (7y). Absences with eyelid myoclonia (9y). Mild ataxia, moderate cognitive impairment. Developmental delay.	trio	high
PME71 Italy	F	***DHDDS***	c.614G>A; p.Arg205Gln (het)	0	unknown	Ataxia (late infancy). Rare TCS (17y), mild action myoclonus (29y). Normal cognition.	singleton	moderate
PME27 Italy	F	***DHDDS***	c.283G>A; p.Asp95Asn (het)	0	unknown	Tremor (21y). Myoclonus (35y), single TCS (36y). Ataxia, normal cognition. Bilateral deafness.	singleton	moderate
PME50 Turkey	F	***ALG10***	c.1170_1171delAA; p.Lys391Valfs*35 (hom)	0	AR	Frequent myoclonus (13y), rare TCS. Ataxia, mild cognitive dysfunction (16y). Scoliosis.	trio	moderate

Abbreviations: MAF – minor allele frequency, AR - autosomal recessive, het – heterozygous, hom – homozygous, gnomAD – The Genome Aggregation Database; TCS – tonic-clonic seizure. Detailed clinical summaries can be found in Table S5. See Methods for criteria for classifying variants as high versus moderate confidence.

Table 2. High and moderate confidence variants identified in established PME genes

Patient ID Country of Origin	Sex	Gene	Variant(s)	gnomAD MAF	Inheritance	Clinical summary (onset age)	WES study design	Confidence
PME83 Australia	M	***SEMA6B***	c.1993delC, p.(Arg665Glyfs*20) (het)	0	AD	Developmental delay and regression. Ataxia, tremor (2.5y). Drop attacks and absence seizures (4y), TCS (11y), wheelchair (11y), multifocal myoclonus (15 y). Severe ID.	singleton[#]	high
PME25 Canada	F	***SEMA6B***	c.2032delG, p.(Glu678Argfs*7)	0	AD	Developmental delay. Ataxia (2.5y). TCS (5y), resting and action myoclonus (10y), possible absence and focal seizures, tremor, wheelchair (14y). Moderate ID.	singleton	moderate
PME15 Italy	F	***CLN6***	c.486+28T>C; intronic (hom)[##]	0	AR	Ataxia (14y). Severe myoclonus (32y), TCS, dementia, pyramidal signs, psychiatric co-morbidities.	singleton	high

PME26 (dec.) Germany	M	***GBA***	c.761+4A>G; splicing (hom)	0	AR	Myoclonus (8y). Ataxia, ophthalmoplegia, mild cognitive impairment, splenomegaly.	singleton	moderate
PME10 Malaysia	M	***NEU1***	c.544A>G, p.(Ser182Gly); deletion of *NEU1* (comp het)	0.001 0	AR	Occasional TCS (12y). Frequent myoclonus (14y), ataxia, normal cognition, normal vision.	trio	high
PME7 Israel	F	***CERS1***	c.210G>A, p.(Trp70*); c.202C>A, p.(Leu68Met) (both hom)	0	AR	Action myoclonus (11/16yr). Ataxia, occasional TCS, mild cognitive impairment.	sibling pair; quartet	high
PME8 Israel	F			0				
PME9 (dec.) Australia	M	***ASAH1***	c.966-2A>G; c.504A>C, p.(Lys168Asn) (comp het)	0.000004 0.00006	AR	Multifocal myoclonus (12y). TCS, progressive limb and bulbar weakness (17y). Hearing impairment (4y). Deceased (19y).	trio	high

Abbreviations: MAF – minor allele frequency, comp het – compound heterozygous, hom - homozygous; AR - autosomal recessive; gnomAD – The Genome Aggregation Database; dec. – deceased; TCS – tonic-clonic seizure. Detailed clinical summaries can be found in Table S5. See Methods for criteria followed when classifying variants as high versus moderate confidence. [#]variant subsequently confirmed *de novo* by Sanger sequencing; maternal DNA did not meet quality control requirements for WES. [##]splicing effect of intronic variant confirmed by RT-PCR (see Figure S4).

Table 3. High and moderate confidence variants identified in established disease genes (not PME)

Patient ID Country of Origin	Sex	Gene	Disease previously associated with Gene	Variant(s)	gnomAD MAF	Inheritance	Clinical presentation	WES study design	Confidence
PME11 Italy	M	***CHD2***	Epileptic encephalopathy, childhood-onset	c.532A>T, p.(Arg178*) (het)	0	*de novo*	Frequent absence seizures and rare TCS (6y), severe myoclonus (14y). Ataxia, dementia. Developmental delay.	trio	high
PME19 Italy	M	***CACNA2D2***	Cerebellar atrophy with seizures and variable developmental delay	c.1260G>A, p.(Thr420=) (het, *de novo*); c.1112A>G, p.(Tyr371Cys) (het, pat inherited)	0 0	AR	Myoclonus, absence and tonic seizures (4y). Dementia, no ataxia. Developmental delay.	trio	high
PME4 (dec.) Italy	F	***STUB1***	Autosomal recessive spinocerebellar ataxia 16; Spinocerebellar ataxia 48	c.169C>T, p.(Pro57Ser) (hom)	0	AR	Ataxia (12y). Myoclonus, TCS (30y). Dementia. Tetraparesis.	trio	high
PME16 Italy	F	***CACNA1A***	Early infantile epileptic encephalopathy; Spinocerebellar ataxia 6; Episodic ataxia type 2; Familial heiplegic migraine 1; Familial hemiplegic migraine 1 with progressive cerebellar ataxia	c.4897G>A, p.(Asp1633Asn) (het)	0	unknown	Ataxia, myoclonus (30y). Cognitive impairment. Sensorineural hearing impairment.	singleton	moderate
PME17 Italy	F	***CAMTA1***	Non-progressive cerebellar ataxia with mental retardation	c.4418G>C, p.(Ser1473Thr) (het)	0.000004	AD	Myoclonus (18y), no TCS. No ataxia or dementia.	parent-child	moderate

PME18 Italy	M						Myoclonus, rare TCS (25y). No ataxia or dementia.		
PME21 Malta	M	***PEX19***	Peroxisome biogenesis disorder 12A (Zellweger)	c.254C>T, p.(Ala85Val) (hom)	0.0009	AR	Progressive ataxia (7yr). Myoclonus, TCS (9y) , dementia (10y). Limb spasticity.	sibling pair	high
PME22 Malta	M						Priogressive ataxia (8y). Myoclonus, TCS (9y). dementia (10y). Limb spasticity.		
PME60 (dec.) Malta	F	***PEX19***	Peroxisome biogenesis disorder 12A (Zellweger)	c.254C>T, p.(Ala85Val) (hom)	0.0009	AR	Progressive severe ataxia (8y). TCS (12y). Hypertonia.	singleton	high
PME5 (dec.) Italy	F	***NAXE***	Encephalopathy, progressive early-onset, with brain oedema and/or leukoencephalopathy	c.128C>A, p.(Ser43*) (hom)	0.00003	AR	Versive motor seizures (12y), daily absence (13y) and myoclonus (15y), rare TCS (21y). Slowly progressive ataxia (19y) dementia and pyramidal signs. Developmental delay.	singleton	high
PME12 Italy	M	***RARS2***	Pontocerebellar hypolasia type 6	c.943C>T, p.(Arg315*); c.425T>C, p.(Val142Ala) (comp het)	0.00004	AR	Mild ataxia (childhood), moderate cognitive impairment. Rare TCS and absence seizures (9y), mild myoclonus (11y).	sibling pair; quartet	moderate
PME13 Italy	F				0.00005		Ataxia (childhood), moderate cognitive impairment. Rare TCS and absence seizures (9), myoclonus (11y).		
PME14 Italy	F	***RARS2***	Pontocerebellar hypolasia type 6	c.1026G>A, p.(Met342Ile); c.3G>A, p.(Met1Ile) (comp het)	0.0002 0	AR	Prominent progressive action myoclonus (25y). No TCS, no ataxia, no dementia.	trio	moderate
PME64 Italy	M	***DYNC1H1***	Charcot-Marie-Tooth disease axonal type 20; Mental retardation, autosomal dominant 13; Spinal muscular atrophy lower extremity-predominant	c.7828delC, p.(Arg2610Glyfs*23) (het)	0	*de novo*	Myoclonus (12y), refractory TCS and absence seizures (22y). No ataxia or dementia.	trio	moderate

Abbreviations: MAF – minor allele frequency; AR - autosomal recessive, comp het – compound heterozygous, het – heterozygous, hom - homozygous; AD – autosomal dominant; gnomAD – The Genome Aggregation Database; dec. – deceased; TCS –tonic-clonic seizure. Detailed clinical summaries can be found in Supplementary Table S5. Please see Methods for criteria followed when classifying variants as high versus moderate confidence. *See Figure S7 for molecular modelling that supports a loss-of-function effect for this *CACNA1A* variant.

Table S1. Major forms of PME with known genetic etiology.

PME subtype	Inheritance pattern	Gene(s)
ULD (EPM1)	AR	*CSTB*
Lafora disease (EPM2A/B)	AR	*EPM2A, NHLRC1*
NCLs	AR	*TPP1, CLN3, CLN5, CLN6, MFSD8, CLN8*
	AD	*DNAJC5*
AMRF (EPM4)	AR	*SCARB2*
North Sea PME (EPM6)	AR	*GOSR2*
MERRF	Mitochondrial	*MT-TK*^
PME (EPM3)	AR	*KCTD7*
Sialidosis type 1	AR	*NEU1*
DRPLA	AD	*ATN1*
MEAK (EPM7)	AD	*KCNC1*
Juvenile Huntingtons	AD	*HTT*
Gaucher disease type 3	AR	*GBA*

^pathogenic variants in this gene accounting for ~90% of MERRF patients

Protein function / molecular pathway
Inhibitor of lysosomal cysteine proteases
Glycogen metabolism
Lysosomal enzymes or membrane proteins
Lysosomal membrane protein
Golgi vesicle transport
Mitochondrial transfer-RNA
Interaction with potassium ion channels
Lysosomal enzyme which breaks down oligosaccharides
Accumulation of ATN1 in neurons due to repeat expansion
Neuronal voltage-gated potassium ion channel
Transcription regulation
Lysosomal enzyme which breaks down glycolipid glucosylceramide

Published >20 independent cases
Yes
Yes
Yes
Yes
Yes
Yes
Yes
Yes
Yes
Yes
Yes
Yes

Table S2. Research variant

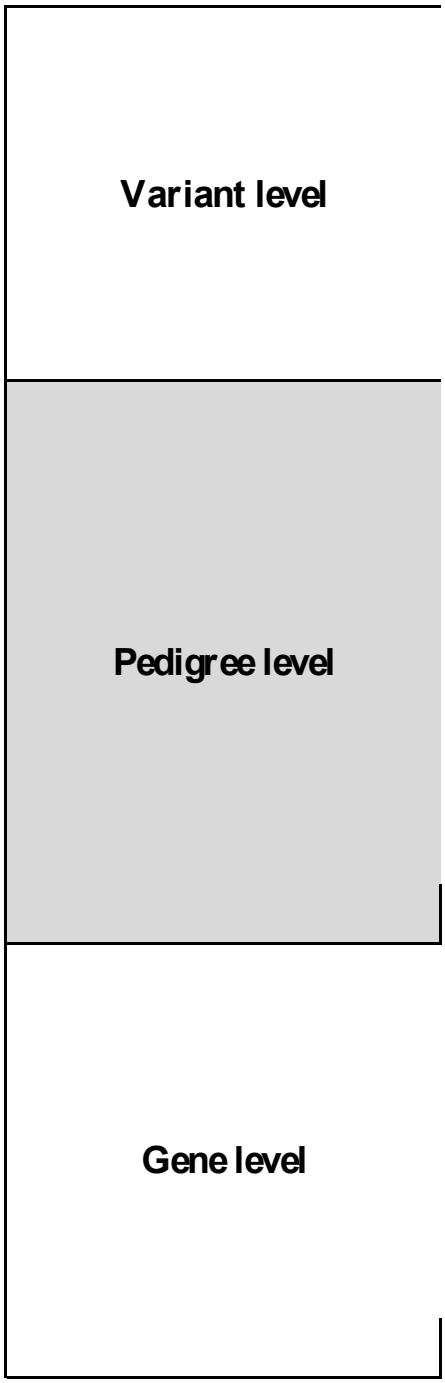

: **prioritisation score**

a) Null variant (nonsense, frameshift, canonical +/- 1 or 2 splice sites, initiation codon, deletion)
b) Damaging missense (all *in silico* tools predict damaging effect)
c) Conflicting missense (at least 1, but not all *in silico* tools predict damaging effect)
d) Splicing variant (all *in silico* tools predict a splicing effect, but variant not at canonical +/- 1 or 2 sites)
e) Inframe deletion
f) Benign missense (all *in silico* tools predict benign effect)
g) Conflicting or benign splicing variant (at least 1 *in silico* tool predicts no splicing effect)
a) Heterozygous *de novo* variant in established dominant disease gene (i.e. parental DNA available)
b) Comp Het variant in established recessive disease gene (i.e. two variants *in trans*)
c) Homozygous variant in established recessive disease gene with pedigree segregation and/or linkage data to support inheritance model
d) Homozygous variant in established recessive disease gene (+/- support with F>0 / variant located in runs of homozygosity RoH)
e) Heterozygous variant in established dominant disease gene inherited from affected parent
f) Heterozygous *de novo* variant in gene with no established disease association
g) Comp Het or homozygous variant in gene with no established disease association
h) Heterozygous variant with undetermined parental inheritance (0.5 if segregation known in single parent)
a) Established PME gene
b) Established neurological gene (e.g., epilepsy, ataxia) with clear patient phenotypic match on clinical review
c) Established neurological gene with overlapping PME features with variants in multiple unrelated patients
d) Established neurological gene (e.g., epilepsy, ataxia) with some patient phenotypic overlap on clinical review
e) Gene has established biological overlap with known PME genes with variants in multiple unrelated patients (0.5 if single patient)
f) Uncertain clinical/biological match with multiple unrelated patients
g) Uncertain clinical/biological match in single patient

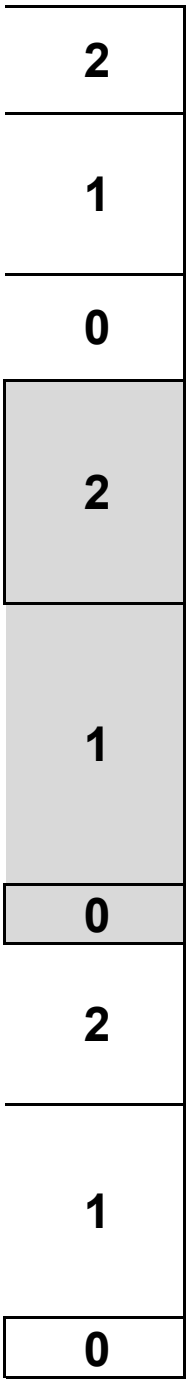
2
1
0
2
1
0
2
1
0

Table S3. Catalogue of short tandem repeats searched for across PME coh

locus	long_name	OMIM	inheritance
DM1	Myotonic dystrophy 1	160900	AD
DM2	Myotonic dystrophy 2	602668	AD
DRPLA	Dentatorubral-pallidoluysian atrophy	125370	AD
EPM1A	Myoclonic epilepsy of Unverricht and Lundborg	254800	AR
FRAXA	Fragile-X site A	309550	X
FRAXE	Fragile-X site E	309548	X
FRDA	Friedreich ataxia	229300	AR
FTDALS1	Amyotrophic lateral sclerosis-frontotemporal dementia	105550	AD
HD	Huntington disease	143100	AD
HDL2	Huntington disease-like 2	606438	AD
SBMA	Kennedy disease	313200	X
SCA1	Spinocerebellar ataxia 1	164400	AD
SCA2	Spinocerebellar ataxia 2	183090	AD
SCA3	Machado-Joseph disease	109150	AD
SCA6	Spinocerebellar ataxia 6	183086	AD
SCA7	Spinocerebellar ataxia 7	164500	AD
SCA8	Spinocerebellar ataxia 8	608768	AD
SCA10	Spinocerebellar ataxia 10	603516	AD
SCA12	Spinocerebellar ataxia 12	604326	AD
SCA17	Spinocerebellar ataxia 17	607136	AD
SCA36	Spinocerebellar ataxia 36	614153	AD
FECD3	Fuchs endothelial corneal dystrophy 3	613267	AD
FAME1	Familial adult myoclonic epilepsy 1	601068	AD
FAME2	Familial adult myoclonic epilepsy 2	607876	AD
FAME3	Familial adult myoclonic epilepsy 3	613608	AD
FAME6	Familial adult myoclonic epilepsy 6	618074	AD
FAME7	Familial adult myoclonic epilepsy 7	618075	AD

ort.

gene	location	gene_region	motif
DMPK	19q13	3'UTR	CTG
ZNF9/CNBP	3q21.3	intron	CCTG
DRPLA/ATN1	12p13.31	coding	CAG
CSTB	21q22.3	promotor	CCCCGCCCCGCG
FMR1	Xq27.3	5'UTR	CGG
FMR2	Xq28	5'UTR	CCG
FXN	9q13	intron	GAA
C9orf72	9p21	intron	GGGGCC
HTT	4p16.3	coding	CAG
JPH3	16q24.3	exon	CTG
AR	Xq12	coding	CAG
ATXN1	6p23	coding	CAG
ATXN2	12q24	coding	CAG
ATXN3	14q32.1	coding	CAG
CACNA1A	19p13	coding	CAG
ATXN7	3p14.1	coding	CAG
ATXN8OS/ATXN8	13q21	utRNA	CTG
ATXN10	22q13.31	intron	ATTCT
PPP2R2B	5q32	promotor	CAG
TBP	6q27	coding	CAG
NOP56	20p13	intron	GGCCTG
TCF4	18q21.2	intron	CTG
SAMD12	8q24	intron	TTTCA
STARD7	2q11.2	intron	TTTCA
MARCHF6	5p15.31-p15.1	intron	TTTCA
TNRC6A	16p12.1	intron	TTTCA
RAPGEF2	4q32.1	intron	TTTCA

Table S4. Summary of lines of evidence data taken into account for all prioritis

ID (manuscript)	chr	base	ref	alt	gene	RefSeq
De novo dominant						
PME1	6	118024815	G	GT	*NUS1*	NM_138459.3
PME2	6	117997141	TG	T	*NUS1*	NM_138459.3
PME11	15	93480836	A	T	*CHD2*	NM_001271.3
PME64	14	102483315	C	-	*DYNC1H1*	NM_001376.4
PME3	1	26784371	G	A	*DHDDS*	NM_024887.3
Heterozygous, presumed dominant						
PME71	1	26784353	G	A	*DHDDS*	NM_024887.3
PME27	1	26769324	G	A	*DHDDS*	NM_024887.3
PME83	19	4544287	G	-	*SEMA6B*	NM_032108.4
PME25	19	4544248	C	-	*SEMA6B*	NM_032108.4
PME16	19	13356049	C	T	*CACNA1A*	NM_001127222.2
PME17, PME18	1	7805952	G	C	*CAMTA1*	NM_015215.4
Homozygous recessive						
PME7, PME8	19	19006672	C	T	*CERS1*	NM_021267.4
PME7, PME8	19	19006680	G	T	*CERS1*	NM_021267.4
PME15	15	68503985	A	G	*CLN6*	NM_017882.3
PME26	1	155207921	T	C	*GBA*	NM_001005742.2
PME4	16	731161	C	T	*STUB1*	NM_005861.4
PME21, PME22	1	160252826	G	A	*PEX19*	NM_001193644.1
PME60	1	160252826	G	A	*PEX19*	NM_001193644.1
PME5	1	156561724	C	A	*NAXE, APOA1BP*	NM_144772.2
PME50	12	34179598	AAA	A	*ALG10*	NM_032834.4
Comp het recessive						
PME9	8	17916975	T	C	*ASAH1*	NM_004315.4
PME9	8	17921967	T	G	*ASAH1*	NM_004315.4
PME10, PME20	6	31829036	T	C	*NEU1*	NM_000434.3
PME10, PME20	6	deletion	.	.	*NEU1*	NM_000434.3
PME19	3	50416523	C	T	*CACNA2D2*	NM_001174051.2
PME19	3	50416903	T	C	*CACNA2D2*	NM_001174051.2

PME12, PME13	6	88234306	G	A	*RARS2*	NM_020320.3
PME12, PME13	6	88258335	A	G	*RARS2*	NM_020320.3
PME14	6	88299673	C	T	*RARS2*	NM_020320.3
PME14	6	88231191	C	T	*RARS2*	NM_020320.3

*score <4, but functional support so "moderate" confidence achieved
^total score the mean average of the two comp het variants scored independently

Abbreviations: CADD - Combined annotation dependent depletion, PolyPhen - Polymorphism phe

ed variants

change	null	annotation	gnomAD	sift
fsIns	yes	c.740dupT, p.(Asp248Glyfs*15)	0	.
fsDel	yes	c.310delG, p.(Val104*)	0	.
stopgain	yes	c.532A>T, p.(Arg178*)	0	.
fsDel	yes	c.7828delC, p.(Arg2610Glyfs*23)	0	.
nsSNV	.	c.632G>A, p.(Arg211Gln)	0	damaging
nsSNV	.	c.614G>A, p.(Arg205Gln)	0	damaging
nsSNV	.	c.283G>A, p.(Asp95Asn)	0	tolerated
fsDel	yes	c.1993delC, p.(Arg665Glyfs*20)	0	.
fsDel	yes	c.2032delG, p.(Glu678Argfs*7)	0	.
nsSNV	.	c.4897G>A, p.(Asp1633Asn)	0	damaging
nsSNV	.	c.4418G>C, p.(Ser1473Thr)	1	damaging
stopgain	yes	c.210G>A, p.(Trp70*)	0	.
nsSNV	.	c.202C>A, p.(Leu68Met)	0	tolerated
unknown	.	c.486+28T>C	0	.
splice intron	.	c.761+4A>G	0	.
nsSNV	.	c.169C>T, p.(Pro57Ser)	0	tolerated
nsSNV	.	c.254C>T, p.(Ala85Val)	130	damaging
nsSNV	.	c.254C>T, p.(Ala85Val)	130	damaging
stopgain	yes	c.128C>A, p.(Ser43*)	7	.
fsDel	yes	c.1170_1171delAA, p.(Lys391Valfs*35)	0	.
splice acceptor	yes	c.966-2A>G	1	.
nsSNV	.	c.504A>C, p.(Lys168Asn)	14	tolerated
nsSNV	.	c.544A>G, p.(Ser182Gly)	26	tolerated
deletion	yes	deletion of NEU1	.	.
splice synonymous	.	c.1260G>A, p.(Thr420=)	0	.
nsSNV	.	c.1112A>G, p.(Tyr371Cys)	0	damaging

stopgain	yes	c.943C>T, p.(Arg315*)	11	.
nsSNV	.	c.425T>C, p.(Val142Ala)	15	tolerated
startloss	yes	c.3G>A, p.(Met1Ile)	0	damaging
nsSNV	.	c.1026G>A, p.(Met342Ile)	69	damaging

enotyping, SIFT - Sorting intolerant from tolerant

polyphen2	CADDv1.5	TraP	Variant score	WES design	variant model
.	35	.	2	trio	heterozygous
.	30	.	2	trio	heterozygous
.	37	.	2	trio	heterozygous
.	35	.	2	trio	heterozygous
probably damaging	33	.	2	trio	heterozygous
probably damaging	33	.	2	singleton	heterozygous
benign	23,3	.	1	singleton	heterozygous
.	26,8	.	2	singleton	heterozygous
.	24,2	.	2	singleton	heterozygous
probably damaging	29,7	.	2	singleton	heterozygous
possibly damaging	26,3	.	2	parent-child pair	heterozygous
.	37	.	2	quartet	homozygous
possible damaging	20,2	.	1	quartet	homozygous
.	1,648	0,72	2	singleton	homozygous
.	22,4	0,934	1	singleton	homozygous
benign	22,6	.	1	trio	homozygous
benign	23		1	sibling pair	homozygous
benign	23		1	singleton	homozygous
.	35		2	singleton	homozygous
.	24,4		2	trio	homozygous
.	29,3	0,57	2	trio	comp het
benign	21,1		1	trio	comp het
benign	23,2		1	trio	comp het
.	.		2	trio	comp het
.	19,64	0,996	1	trio	comp het
probably damaging	28,6	.	2	trio	comp het

.	44		2	quartet	comp het
benign	18,11		0	quartet	comp het
benign	23	.	1	trio	comp het
benign	25,2		1	trio	comp het

inheritance/segregation	Fest	RoH support	Pedigree score	Functional support
de novo	0	n/a	2	yes
de novo	0	n/a	2	yes
de novo	0	n/a	2	
de novo	0	n/a	2	
de novo	0	n/a	2	yes
unknown	0	n/a	0	yes
unknown (absent in father)	0	n/a	0,5	yes
de novo	0	n/a	2	
unknown	0	n/a	0	
unknown	0	n/a	0	
dominant	0	n/a	1	
recessive	0,08	yes	2	
recessive	0,08	yes	2	
recessive	0,035	yes	1	
recessive	0,012	yes	1	
recessive	0,18	yes	2	
recessive	0,027	yes	2	
recessive	0	yes	2	
recessive	0	.	1	
recessive	0,12	yes	2	yes
recessive (pat.)	0	n/a	2	
recessive (mat.)	0	n/a	2	
recessive (mat.)	0	n/a	2	
recessive (pat.)	0	n/a	2	
recessive (de novo)	0	n/a	2	
recessive (pat.)	0	n/a	2	

recessive (pat.)	0	n/a	2
recessive (mat.)	0	n/a	2
recessive (mat.)	0	n/a	2
recessive (pat.)	0	n/a	2

Functional notes	Gene-disease ass	Gene score		Total score
patient-derived fibroblasts - immunoblotting, cis-PT activity, filipin staining	DEE	2		6
patient-derived fibroblasts - immunoblotting, cis-PT activity, filipin staining	DEE	2		6
	DEE	1		5
	Complex neurological	0		4
yeast deletion strain	DEE	2		6
yeast deletion strain and patient-derived fibroblasts	DEE	2		4
yeast deletion strain and patient-derived fibroblasts	DEE	2		3,5
	PME	2		6
	PME	2		4
	Ataxia; DEE	2		4
	Ataxia	1		4
	PME	2		6
	PME	2		5
	PME	2		5
	PME	2		4
	Ataxia	2		5
	Complex neurological	2		5
	Complex neurological	2		5
	Complex neurological	2		5
yeast deletion strain, glycosylation test from patient-derived fibroblasts	n/a	0,5		4,5
	PME	2	6	5,5
	PME	2	5	
	PME	2	5	5,5
	PME	2	6	
	DEE	1	4	4,5
	DEE	1	5	

Complex neurological	1	5	4
Complex neurological	1	3	
Complex neurological	1	4	4
Complex neurological	1	4	

Overall confidence	Muona *et al.* 2015	ACMG criteria met
high	.	PVS1, PM2, PM6, PP4
high	.	PVS1, PM2, PM6, PP4
high	.	PVS1, PS2, PM2, PP3
moderate	yes	PVS1, PM2, PM6, PP4
high	.	PS1, PS2, PS3, PM1, PM2, PP2, PP3,
moderate	.	PS3, PM1, PM2, PP2, PP3, PP5
moderate*	.	PM2, PP3, PP4
high	.	PVS1, PM2, PM6
moderate	.	PVS1, PM2
moderate	.	PM1, PM2, PP3, PP5
moderate	.	PM2, BP1
high	.	PVS1, PM2, PP1, PP3, PP4
high	.	PM2, PM3, PP1, PP2, PP4, BP4
high	.	PM2, PM3, PP4, BP4
moderate	.	PM2, PM3, PP4, BP4
high	.	PM1, PM2, PP2
high	.	PM2, PP3, PP4, BP1
high	yes	PM2, PP3, PP4, BP1
high	yes	PVS1, PM3, PP3, PP4
moderate	yes	PM2, PM3, PP4
high^	.	PVS1, PM2, PM3, PP3, PP4
	.	PM1, PM2, PM3, PP4, PP5
high^	.	PM1, PM2, PM3, PP1, PP4, PP5
	.	.
high^	.	PS2, PM2, PM3, PP3
	.	PM1, PM2, PM3, PP3, BP1

moderate^	.	PVS1, PM2, PP3, PP5
	.	PM1, PM2, PM3
moderate^	.	PM2, PP3
	.	PM1, PM2, PP3

ACMG classification

Pathogenic

Pathogenic
Pathogenic
Pathogenic
Pathogenic

Pathogenic

Uncertain significance
Pathogenic
Likely Pathogenic
Likely Pathogenic
Uncertain significance

Pathogenic
Likely Pathogenic
Likely Pathogenic
Uncertain significance
Uncertain significance
Uncertain significance
Uncertain significance
Pathogenic

Uncertain significance

Pathogenic
Likely Pathogenic
Likely Pathogenic
.
Pathogenic
Likely Pathogenic

Pathogenic
Likely Pathogenic
Uncertain significance
Uncertain significance

Table S5. Clinical summary for patients with causative or likely ca

Patient ID	Gene	Disease associated to the gene (Phenotype MIM number, if available)
Established PME genes		
PME83	*SEMA6B*	PME
PME25	*SEMA6B*	PME
PME7, PME8	*CERS1*	PME (616230)
PME9	*ASAH1*	PME: Spinal muscular atrophy with progressive myoclonic epilepsy (159950)
PME26	*GBA*	PME: Gaucher Disease (231000)
PME10	*NEU1*	PME: Sialidosis type I (256550)
PME15	*CLN6*	PME: Neuronal Ceroid Lipofuscinosis, Kufs type adult onset (204300)
Established epilepsy (but not PME) genes		

PME1	*NUS1*	Congenital disorder of glycosylation type Iaa (617082), Autosomal dominant Mental Retardation 55 with seizures (617831). PME phenotype previously reported in case report
PME2	*NUS1*	Congenital disorder of glycosylation type Iaa (617082), Autosomal dominant Mental Retardation 55 with seizures (617831). PME phenoptype previously reported in case report
PME3	*DHDDS*	Developmental delay and seizures with or without movement abnormalities (617836), Congenital disorder of glycosylation type Ibb (613861). Retinitis Pigmentosa 59 (613861). PME not previously described
PME71	*DHDDS*	Developmental delay and seizures with or without movement abnormalities (617836), Congenital disorder of glycosylation type Ibb (613861). Retinitis Pigmentosa 59 (613861). PME not previously described
PME27	*DHDDS*	Developmental delay and seizures with or without movement abnormalities (617836), Congenital disorder of glycosylation type Ibb (613861). Retinitis Pigmentosa 59 (613861). PME not previously described
PME19	*CACNA2D2*	Cerebellar atrophy with seizures and variable developmental delay (618501). PME not previously described
PME11	*CHD2*	Epileptic encephalopathy, childhood-onset (615369). PME not previously described
Established ataxia genes		
PME4	*STUB1*	Autosomal recessive spinocerebellar ataxia 16 (615768), Spinocerebellar ataxia 48 (618093). PME not previously described

PME16	*CACNA1A*	Early infantile epileptic encephalopathy (617106), Spinocerebellar ataxia 6 (183086), Episodic ataxia type 2 (108500), Familial heiplegic migraine 1 (141500), Familial hemiplegic migraine 1 with progressive cerebellar ataxia (141500). PME not previously described
PME17, PME18	*CAMTA1*	Non-progressive cerebellar ataxia with mental retardation (614756). PME not previously described
Established other neurological disease genes		
PME5	*NAXE*	Encephalopathy, progressive early-onset, with brain oedema and/or leukoencephalopathy (617186). PME not previously described
PME21, PME22	*PEX19*	Peroxisome biogenesis disorder 12A (Zellweger) (614886). PME not previously described
PME60	*PEX19*	Peroxisome biogenesis disorder 12A (Zellweger) (614886). PME not previously described
PME64	*DYNC1H1*	Charcot-Marie-Tooth disease axonal type 20 (614228), Mental retardation, autosomaldominant 13 (614563), Spinal muscular atrophy lower extremity-predominant (158600). PME not previously described

PME12, PME13	*RARS2*	Pontocerebellar hypolasia type 6 (611523). PME previously reported in case series
PME14	*RARS2*	Pontocerebellar hypolasia type 6 (611523). PME previously reported in case series
Novel disease gene		
PME50	*ALG10*	No known neurological disease associations

ıusative genetic variants identified in this study.

Confirmed or presumed inheritance	Ancestry	Consanguinity	Sex	Category
de novo dominant (confirmed)	Australian	no	M	DD + PME
de novo dominant (presumed)	Canadian	no	F	DD + PME
autosomal recessive (confirmed; homozygous)	Sephardic	yes	F, F	ULD-like
autosomal recessive (confirmed; comp het)	Australian (Italian)	no	M	ULD-like
autosomal recessive (confirmed; homozygous)	Turkish	yes	M	ULD-like
autosomal recessive (confirmed; comp het)	Malaysian	no	M	ULD-like
autosomal recessive (confirmed; homozygous)	Italian	yes	F	PME + dementia

de novo dominant (confirmed)	Italian	no	M	ULD-like
de novo dominant (confirmed)	Italian	no	F	PME + dementia
de novo dominant (confirmed)	Italian	no	M	DD + PME
de novo dominant (presumed)	Italian	no	F	ULD-like
de novo dominant (presumed)	Italian	no	F	Late onset
autosomal recessive (confirmed; comp het)	Italian	no	M	DD + PME
de novo dominant (confirmed)	Italian	no	M	DD + PME
autosomal recessive (confirmed; homozygous)	Italian	yes	F	PME + dementia

autosomal dominant (presumed)	Italian	no	F	Late onset
autosomal dominant (confirmed)	Italian	no	M.F	ULD-like/Late onset
autosomal recessive (presumed; homozygous)	Italian	no	F	PME + DD
autosomal recessive (confirmed; homozygous)	Maltese	yes	M,M	PME + dementia
autosomal recessive (confirmed; homozygous)	Maltese	no	F	PME + dementia
de novo dominant (confirmed)	Italian	no	M	ULD-like

autosomal recessive (confirmed; comp het)	Italian	no	M,F	PME + dementia
autosomal recessive (confirmed; comp het)	Italian	no	F	Late onset
autosomal recessive (presumed; homozygous)	Turkish	yes	F	PME + dementia

Clinical summary
Developmental delay. Late walker and always unstaedy with tremor. Ataxia (approx 2.5y). Drop attacks and absence seizures (4y); TCS (11y); Wheelchair (11y);. Severe generalised and multifocal myoclonus (15y); myoclonic status. Slow cognitive regression from 5y. Severe intellectual disability. No pyramidal signs and head circumference normal. Alive age 37y.
Developmental delay. Walked independently at 2y; unsteady wide gait noted at 2.5y. Generalized epileptiform discharges recorded at 2.5yr. First TCS at 5y during illness. Recurrent convulsions some with a focal component. Resting and action myoclonus noted at 10y. Tremor. Increasing difficultly with gait from 11y; wheelchair by 14y. Dysarthria noted at 16y. Moderate intellectual disability; no definitive cognitive decline. No pyramidal signs and head circumference on 50th centile. Alive at 39y.
Sibling pair. PME7 febrile seizure at 6m. Learning difficulties noted at 3.5y. PME onset at 11y with rare TCS. Moderately severe action and rest myoclonus and ataxia from 13y. Cognitive decline. EEG: irregular GSW and polyspike + photosensitivity. PME8 normal development and early education. Memory problems noted from secondary school. Moderate myoclonus and ataxia from 16y. Rare TCS, dysarrthria. EEG: irregular GSW and polyspike + photosensitivity.
Onset age 12 of TCS and multifocal action and rest myoclonus, on a background of normal development and early severe hearing impairment (4y) . Subsequent progressive limb and bulbar weakness. Rapidly progressive, death age 19.

Onset age 8 of myoclonus. Associated with ataxia, horizontal gaze palsy, mild splenomegaly and mild intellectual disability. Progressive course, death age 19.

Onset 12 years of infrequent TCS on background of normal development. Frequent myoclonus from 14 years, progressive ataxia. Normal vision and normal fundus examination. Normal cognition.
Onset age 14 of ataxia. Severe myoclonus from age 32, TCS, moderate dementia. Dysphagia and pyramidal signs noted. Psychiatric co-morbidities. Severe cerebral, moderate cerebellar atrophy. EEG: photoparoxysmal response.

Onset age 13 of frequent rest and action myoclonus, on background of mild learning difficulties. No seizures or ataxia. Normal cognition.
Onset age 4 of febrile seizure and subsequent developmental regression. Daily absence seizures, associated with eyelid myoclonus from 4 years of age and upper limb myoclonus at 8 years of age. Stable ataxia, moderate cognitive decline noted. MRI: cerebellar atrophy.
Onset age 7 slowly progressive myoclonus, ataxia on a background of developmental delay. Absence with eyelid myoclonia from age 9. No TCS. Moderate cognitive impairment.
Onset in late infancy of ataxia (mild and non-progressive), then TCS from age 17 and mild action myoclonus noted age 29. Mild learning difficulties in childhood, normal cognition. MRI: mild cerebral, cerebellar and brainstem atrophy.
Onset age 21 of tremor, daily myoclonus from 35 years of age, slowly progressive ataxia from 37 years of age. Single TCS. Normal developmental history, normal cognition. Multiple co-morbidities including bilateral deafness, cataracts, retinal dystrophy, dolicocolon, atonic bladder, hashimoto's thyroiditis, polycystic kidney disease. MRI: cerebellar atrophy.
Onset 4 years of age of myoclonus, absence and tonic seizures on background of developmental delay. Myoclonic tremor and upper limb dystonic posturing from 30 years of age. No ataxia reported. Dementia. MRI: cerebellar atrophy.
Onset age 6 of frequent absence seizures, occasional TCS and myoclonus on background of developmental delay. Severe, progressive myoclonus, ataxia and cognitive decline from age 15. Abnormal eye movements and mild extrapyramidal signs noted. History of psychosis and autism. EEG: GSW and PPR.
Onset 12 years of age with ataxia. Myoclonus and occsional TCS from age 30. Severe action and reflex myoclonus, severe progressive ataxia and slowly progressive dementia. Tetraparesis and bilateral pes cavus noted.

Progressive ataxia from 30 years of age (possible childhood onset) associated with myoclonus, on a background of mild intellectual impairment and sensorineural hearing impairment. MRI showing cerebellar atrophy and EEG findings of diffuse paroxysmal abnormalities consistent with encephalopathy. No migraine. Family history of epilepsy and possible ataxia affecting father and brother (now deceased).
Father-daughter pair. Daughter age of onset 18 years with myolonus; no other seizure types. Father with adult onset rare TCS and mild myoclonus. Both on a backround of normal development, with no cognitive impairment or ataxia.
Onset age 12 of versive motor seizures on background of developmental delay (at onset EEGs were suggestive of Lafora or mitochondrial disease, as they showed bi-occipital spiking that was suppressed by eye opening, generalized spikes and strong photosensitivity). Absence seizures from 13 years, daily myoclonus from 15 years. Occasional TCS. Slowly progressive severe ataxia, Dementia. Abnormal eye movements, hyper-reflexia, bilateral Hoffman's and Babinski reflexes, mild extrapyramidal signs. Brain MRI as well as muscle and skin biopsy were unremarkable. Death at 26 years due to refractory myoclonic status.
Sibling pair, both with a history of developmental delay presenting at 7 and 8 years of age with progressive ataxia, occasional myoclonus and TCS and dementia. Associated with limb spasticity.
Onset age 8 ataxia, then TCS from age 12, on a background of normal developmental history prior to onset. Progressive severe ataxia. Hypertonia noted. Death age 35. (Affected brother not recruited)
Onset age 12 of multifocal action and rest myoclonus. Frequent TCS and absence seizures refractory to medication from 22 years of age. No ataxia, normal cognition. Moderate dysarthria.

Sibling -pair with childhood onset mild progressive ataxia, mild predominantly upper limb action myoclonus, occasional TCS and absence seizures. Childhood onset cognitive impairment diagnosed prior to onset of myoclonus and ataxia. MRI unremarkable.
Onset 25 years of prominent progressive action myoclonus. Normal developmental history, normal cognition. No ataxia, no TCS. Scoliosis and ovarian insufficiency.
Onset age 13 of frequent action and reflex myoclonus on a background of normal development. Slowly progressive ataxia and mild cognitive dysfunction noted from age 16. Two isolated TCS. Scoliosis, obesity.

Summary of the genetic finding / clinical fit
The patient's electroclinical phenotype is consistent with the recent report of PME due to pathogenic variants in *SEMA6B* . The frameshift variant identified in this patient and subsequently confirmed *de novo* is located within the same last exon of all previously reported cases. Thus, the phenotype is compatible for the genetic finding.
The patient's electroclinical phenotype is consistent with the recent report of PME due to pathogenic variants in SEMA6B. The frameshift variant identified in this patient is located within the same last exon of all previously reported cases. Whilst the phenotype is compatible with *SEMA6B* mutation, in the absence of parental DNA to confirm the variant as *de novo* we remain cautious and report this finding with moderate confidence.
The patients' electrolinical phenotype is consistent with the previous reports of PME due to pathogenic variant in *CERS1* . The parents are related, consistent with the homozygous variant that is ultra-rare and predicted damaging. Thus, the phenotype is compatible with the genetic finding.
The patient's electroclinical phenotype is consistent with previous reports of SMA-PME due to pathogenic variants in *ASAH1.* The parents are not related, consistent with the bi-allelic autosomal recessive inheritance of two rare damaging variants in this established PME gene. Thus, the phenotype is compatible with the genetic finding.
The patient's electrolinical phenotype is consistent with previous reports of PME due to pathogenic variant in *GBA.* The parents are related, consistent with the homozygous splicing variant that is ultra-rare and predicted damaging. The phenotype is highly suggestive of Gaucher disease and *in silico* tools unanimously predict a splicing effect in GBA. However in the absence of experimental confirmation we remain cautious and predict this finding with moderate confidence.
The patient's electrolinical phenotype is consistent with previous reports of PME due to pathogenic variant in *NEU1.* Although no cherry red spot was present, the absence of this has now been reported in a number of independent cases. The parents are not related, consistent with the bi-allelic autosomal recessive inheritance of two rare damaging variants in this established PME gene. Thus, the phenotype is compatible with the genetic finding.
The patient's electroclinical phenotype is consistent with previous reports for *CLN6* . The parents are related, consistent with the novel homozygous intronic variant. The phenotype is compatible with *CLN6* mutation and RNA level studies with RT-PCR and sequencing have confirmed the variant results in aberrant splicing, thus we report this finding with high confidence.

Although the patient has later age at onset, intact cognition and no scoliosis, the electroclinical phenotype shares some features with those previously reported for this gene, with **prominent myoclonus**. The novel frameshift variant is confirmed *de novo* and functional studies support the damaging *in silico* predications. Thus, it is with high confidence we establish NUS1 as a new PME gene.
The patient's electroclinical phenotype is consistent with previous reports for this gene, with **early childhood onset myoclonus, subsequent cognitive decline and cerebellar atrophy**. The novel frameshift variant is confirmed *de novo* and functional studies support the damaging *in silico* predications. Thus, it is with high confidence we establish *NUS1* as a new PME gene.
The patient's electroclinical phenotype is similar to previous reports for this gene, notably onset of **myoclonus** and **ataxia** in the first decade of life on a background of **global developmental delay**. The confirmed *de novo* has been reported previously as pathogenic in a patient with developmental and epileptic encephalopathy and our functional studies support the damaging *in silico* predications. It is therefore with high confidence that we expand the *DHDDS* clinical spectrum to PME.
Although there is no history of developmental delay, the patient's electroclinical phenotype shares several other features with previous reports for this gene, including **early onset ataxia** and **subsequent myoclonus**. Functional studies support the damaging *in silico* predications for this novel variant, but without parental DNA samples to confirm *de novo* status, we remain cautious and report this finding with moderate confidence.
The patient's electroclinical phenotype shares some features with previous reports for this gene, namely **ataxia** and **myoclonus**. However onset is considerably later, and there is no history of developmental delay. Whilst functional studies support a damaging effect for this novel variant, but with a maternal DNA sample to confirm *de novo* status, we remain cautious and report this finding with moderate confidence.
The patient's electroclinical phenotype shares several features with previous reports for this gene; **cerebellar atrophy, developmental delay and hyperkinetic movements** are consistent, although later age at onset is noted. The two ultra-rare predicted damaging variants were confirmed *in trans* and the parents are not related, consistent with the bi-allelic autosomal recessive inheritance. Thus, it is with high confidence we expand the *CACNA2D2* clinical spectrum to PME.
The patient's electro-clinical phenotype, **with prominent photosensitivity in particular**, has overlapping features with what has previously been reported for *CHD2.* The novel stop variant is confirmed *de novo* and thus it is therefore with **high** confidence we expand the *CHD2* clinical spectrum to PME.

The patient's clinical phenotype shares a number of features with previous reports for this gene, notably onset of **prominent ataxia** in the second decade, with myoclonus and **cognitive impairment**. The parents are related, consistent with the ultra-rare variant being homozygous. It is therefore with **high** confidence that we expand the *STUB* phenotype to PME.

The patient's electroclinical phenotype shares features with what has previously been reported for this gene, notably **progressive ataxia**. The positive autosomal **dominant family history** is consistent with this **ultra-rare, heterozygous predicted damaging missense variant** being causative. It is therefore with moderate confidence that we expand the *CACNA1A* clinical spectrum to PME.
The patients' electroclinical phenotype has little overlap with previous reports for this gene, with no evidence of ataxia or cognitive impairment. However, the **confirmed autosomal dominant inheritance** is consistent with this **ultra-rare, predicted damaging** variant being causative. It is therefore with moderate confidence that we expand the *CAMTA1* clinical spectrum to PME.

The patient's electroclinical phenotype shares some features with previous reports for this gene, notably **developmental delay** and **subacute ataxia**. Features which are not consistent include later onset, a less rapidly progressive clinical course and no evidence of cerebral oedema. The confirmed autosomal recessive inheritance of this **rare stopgain variant** is consistent with this presumed homozygous variant being causative. It is therefore with high confidence we expand the *NAXE* clinical spectrum to PME.
The sib-pair's electroclinical phenotype is different to the previously reported phenotype in a single case, with childhood onset, no dysmorphic features and a less rapidly progressive clinical course. However, the same predicted damaging missense variant is homozygous in four unrelated families (two reported here) with similar presentation from Malta; the same haplotype was confirmed supporting a **founder effect.** The variant was not present in the Maltese human genome project (n=400). It is therefore with high confidence we expand the *PEX19* clinical spectrum to PME.
The sib-pair's electroclinical phenotype is different to the previously reported phenotype in a single case, with childhood onset, no dysmorphic features and a less rapidly progressive clinical course. However, the same predicted damaging missense variant is homozygous in four unrelated families (two reported here) with similar presentation from Malta; the same haplotype was confirmed supporting a **founder effect.** The variant was not present in the Maltese human genome project (n=400). It is therefore with high confidence we expand the *PEX19* clinical spectrum to PME.
The patient's electro-clinical phenotype has little to no overlap with what has been previously reported for this gene. However, the **novel frameshift variant is confirmed *de novo*** and it is therefore with moderate confidence we expand the *DYNC1H1* clinical spectrum to PME.

The patients' electroclinical phenotype shares some features (**ataxia, myoclonus and cognitive impairment**) with previous case reports for this gene, although onset is later (childhood, not infantile), and other associated features (extrapyramidal features, oculomotor apraxia) are not noted. The two ultra-rare predicted damaging variants were confirmed in trans and the parents are not related, consistent with the bi-allelic autosomal recessive inheritance. It is therefore with **moderate** confidence that we expand the *RARS2* phenotype to PME.

The patient's electroclinical phenotype shares some features with previous reports for this gene, namely prominent **myoclonus**, though later onset (not infantile) and a lack of other associated features is noted. The two ultra-rare predicted damaging variants were confirmed in trans and the parents are not related, consistent with the bi-allelic autosomal recessive inheritance. It is therefore with **moderate** confidence that we expand the *RARS2* phenotype to PME.

There are no previous reports of neurological disease associated with *ALG10* pathogenic variants. However, the **novel homozygous frameshift variant** is consistent with the confirmation that the **parents are related**. **Functional studies support** the damaging *in silico* prediction for the variant and the gene is biologically highly plausible as a **member of the same glycosylation pathway as *NUS1* and *DHDDS*** . In the absence of a second unrelated patient with a variant in this gene, we remain cautious and report the variant as pathogenic and *ALG10* as a new PME gene with moderate confidence.

Overall confidence level
High
Moderate
High
High
Moderate
High
High

High
High
High
Moderate
Moderate
High
High
High

Moderate
Moderate
High
High
High
Moderate

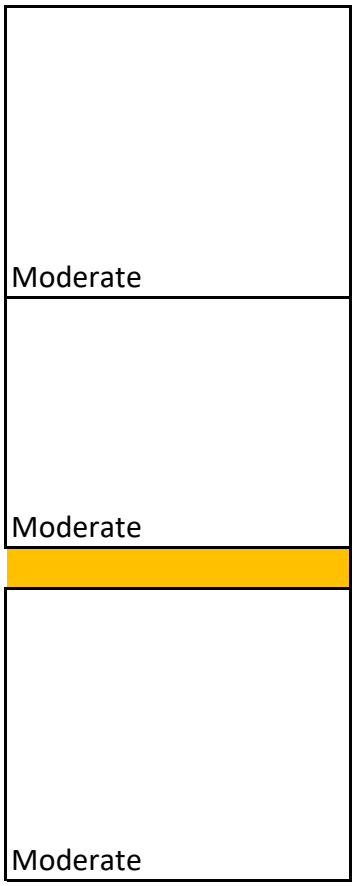
Moderate
Moderate
Moderate

Table S6. Summary of lines of evidence data taken into accou

ID	chr	base	ref	alt	gene	change
PME27	19	10265606	T	C	*DNMT1*	nsSNV
PME50	12	38714351	A	C	*ALG10B*	nsSNV
PME54	10	101996698	G	A	*CWF19L1*	nsSNV
PME_FI_E04	7	129756345	A	G	*KLHDC10*	nsSNV
PME_FI_F01	1	1464680	G	A	*ATAD3A*	nsSNV
PME_FI_C07	1	202698866	G	C	*KDM5B*	nsSNV
PME_FI_C07	6	26156805	A	C	*HIST1H1E*	nsSNV
PME_FI_F04	2	68365900	G	A	*WDR92*	nsSNV
PME_FI_G07,	2	166894429	T	A	*SCN1A*	nsSNV
PME_FI_H02	20	62038227	C	T	*KCNQ2*	nsSNV
PME_FI_B10	10	93601167	G	A	*TNKS2*	nsSNV
PME_FI_F07	12	72893404	G	A	*TRHDE*	nsSNV
PME_FI_F07	13	100635052	G	C	*ZIC2*	nsSNV
PME_FI_F04	9	33294540	TCAC	T	*NFX1*	inframeDel
PME_FI_G07,	2	166859087	A	T	*SCN1A*	nsSNV
PME_FI_H02	10	64966847	T	G	*JMJD1C*	nsSNV
PME54	17	42428728	C	T	*GRN*	splicing
PME_FI_B10	6	27278397	T	C	*POM121L2*	nsSNV
PME_FI_D10	22	20939408	G	A	*MED15*	nsSNV
PME_FI_G04	6	24456817	T	C	*GPLD1*	nsSNV
PME_FI_C04	1	160054663	A	G	*KCNJ9*	sSNV; splicing
PME_FI_C04	15	56719823	C	A	*TEX9*	nsSNV
PME_FI_F04	4	187077187	G	T	*FAM149A*	nsSNV
PME48	15	93518188	A	G	*CHD2*	splicing
PME_FI_G12	3	53765148	A	G	*CACNA1D*	nsSNV

Abbreviations: CADD - Combined annotation dependent depletion, PolyPh

ınt for variants that did not meet the prioritisation criteria

annotation	RefSeq	gnomAD count	null	sift
c.1619A>G, p.(Tyr540Cys)	NM_001130823.1	0	.	damaging
c.758T>G, p.(Leu253Trp)	NM_001013620.3	0,004		damaging
c.1283C>T, p.(Thr428Ile)	NM_018294.6	1	.	tolerated
c.314A>G, p.(Tyr105Cys)	NM_014997.3	0	.	damaging
c.1727G>A, p.(Arg576Gln)	NM_018188.3	0	.	damaging
c.4574C>G, p.(Ala1525Gly)	NM_006618.3	0	.	damaging
c.187A>C, p.(Lys63Gln)	NM_005321.2	0	.	damaging
c.607C>T, p.(Arg203Trp)	NM_138458.4	6	.	damaging
c.2803A>T, p.(Asn935Tyr)	NM_001165963.2	0	.	damaging
c.2389G>A, p.(Glu797Lys)	NM_172107.2	0	.	damaging
c.1801G>A, p.(Ala601Thr)	NM_025235.4	0	.	tolerated
c.1576G>A, p.(Ala526Thr)	NM_013381.2	1	.	damaging
c.734G>C, p.(Arg245Pro)	NM_007129.3	0	.	damaging
c.153_155delACC, p.(Pro53del)	NM_002504.6	0	.	.
c.4179T>A, p.(His1393Gln)	NM_001165963.2	0	.	tolerated
c.4882A>C, p.(Ser1628Arg)	NM_032776.3	0	.	damaging
c.836-3C>T	NM_002087.3	3	.	.
c.1553A>G, p.(His518Arg)	NM_033482.3	0	.	tolerated
c.1985G>A, p.(Arg662Gln)	NM_001003891.1	1	.	tolerated
c.1057A>G, p.(Met353Val)	NM_001503.4	2	.	tolerated
c.843A>G, p.(Glu281=)	NM_004983.2	0	.	.
c.984C>A, p.(His328Gln)	NM_198524.2	0	.	tolerated
c.417G>T, p.(Gln139His)	NM_015398.2	0	.	tolerated
c.2577+8A>G	NM_001271.3	0	.	.
c.2441A>G, p.(Asn814Ser)	NM_000720.3	0	.	tolerated

ɐn - Polymorphism phenotyping, SIFT - Sorting intolerant from tolerant

polyphen2	CADDv1.5	TraP	model	inheritance	ACMG criteria met
probably damaging	24,8	.	heterozygous	unknown	PM1, PM2, PP3
probably damaging	19,8		homozygous	recessive	BS1
benign	14,35	.	homozygous	recessive	PM2, BP4
probably damaging	28,1	.	heterozygous	de novo	PS2, PM2, PP3
possibly damaging	25,7	.	heterozygous	de novo	PS2, PM2, PP3
probably damaging	31	.	heterozygous	de novo	PS2, PM2, PP3
probably damaging	28,6	.	heterozygous	de novo	PS2, PM2, PP3
possibly damaging	28,4	.	homozygous	recessive	PM3, PP3, PP4
benign	15,92	.	comp het	recessive	PM1, PM2, BP4
possibly damaging	33	.	heterozygous	unknown	PM2, PP3
probably damaging	24,4	.	heterozygous	de novo	PS2, PM2, PP3
benign	23,1	.	heterozygous	de novo	PS2, PM2, PP3
benign	26,6	.	heterozygous	de novo	PS2, PM1, PM2, PP2, PP3
.	17,16	.	homozygous	recessive	PM2, PM3, PM4
benign	11,42	.	comp het	recessive	PM1, PM2, BP4
probably damaging	22	.	heterozygous	unknown	PM2, PP3, BP1
.	15,22	0,48	heterozygous	unknown	PM2, BP4
benign	5,838	.	heterozygous	de novo	PS2, PM2, BP4
benign	23,6	.	heterozygous	de novo	PS2, PM2, PP3
benign	0,084	.	heterozygous	de novo	PS2, PM2, BP4
.	13,02	0,12	heterozygous	de novo	PS2, PM2, BP7
benign	0,373	.	heterozygous	de novo	PS2, PM2, BP4
benign	0,09	.	homozygous	recessive	PM2, PM3, PP4, BP4
.	10,1	0,05	heterozygous	unknown	PM2, BP4
benign	21,8	.	heterozygous	unknown	PM2, BP4

ACMG classification	**Sanger validated**	**Muona *et al.***	**Variant score**
Uncertain significance	yes	.	2
Uncertain significance	yes		2
Uncertain significance	no	.	0
Likely pathogenic	no	.	2
Likely pathogenic	no	.	2
Likely pathogenic	no	.	2
Likely pathogenic	no	.	2
Uncertain significance	no	.	2
Uncertain significance	yes	.	1
Uncertain significance	yes	.	2
Likely pathogenic	no	.	1
Likely pathogenic	no	.	1
Pathogenic (likely pathogenic)	no	.	1
Uncertain significance	no	.	1
Uncertain significance	yes	.	0
Uncertain significance	no	.	2
Uncertain significance	no	.	1
Likely pathogenic	no	.	0
Likely pathogenic	no	.	0
Likely pathogenic	no	.	0
Likely pathogenic	no	.	0
Likely pathogenic	no	.	0
Uncertain significance	no	.	0
Uncertain significance	no	.	0
Uncertain significance	no	.	0

Pedigree score	Gene score	Total score
0,5	1	3,5
1	0	3
2	1	3
1	0	3
1	0	3
1	0	3
1	0	3
1	0	3
1	1	3
0	1	3
1	0	2
1	0	2
1	0	2
1	0	2
1	1	2
0	0	2
0	1	2
1	0	1
1	0	1
1	0	1
1	0	1
1	0	1
1	0	1
0	1	1
0	0	0

Supplemental Data

Tables S1-S6

- S1: Major forms of PME with known genetic etiology
- S2: Research variant prioritization score
- S3: Catalogue of short tandem repeats searched for across PME cohort
- S4: Summary of lines of evidence data taken into account for all prioritized variants
- S5: Clinical summary for patients with causative or likely causative genetic variants identified in this study
- S6: Summary of lines of evidence data taken into account for variants that did not meet the prioritization criteria

Figures S1-S7

- S1: Age of PME onset distribution for all 78 unrelated probands.
- S2: Pathogenic variants in *NUS1*, *DHDDS* and *ALG10* and dolichol-dependent glycosylation pathway.
- S3: IGV snapshot of the two *SEMA6B* frameshift variants demonstrating low coverage.
- S4: Aberrant splicing caused by the deep intronic *CLN6* variant.
- S5: Deletion confirmation of NEU1 was performed by quantitative PCR
- S6: Chr1q23.2 haplotype encompassing *PEX19* c.254C>T (p.A85V) variant.
- S7: Molecular modelling supports *CACNA1A* variant loss-of-function effect.

Figure S1. **Age of PME onset distribution for all 78 unrelated probands.**

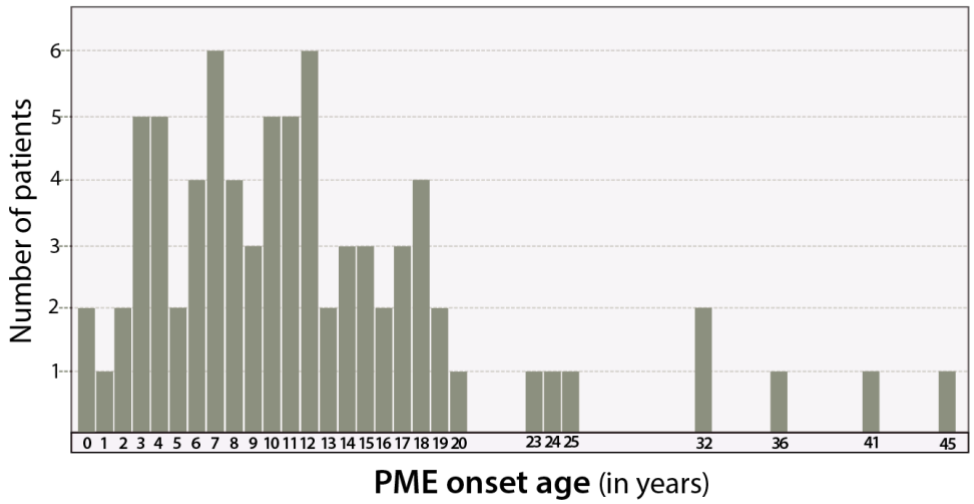

Figure S2. **Pathogenic variants in *NUS1*, *DHDDS* and *ALG10* and dolichol-dependent glycosylation pathway.** (**A**) Locations of variants in *NUS1*. (**B**) Locations of variants in *DHDDS*. (**C**) Locations of variant in *ALG10.* (**D**) Glycosylation pathway showing involvement of NUS1, DHDDS and ALG10 (in red) (adapted from Stanley P, Taniguchi N, Aebi M. N-Glycans. In: Varki A, Cummings RD, Esko JD, Stanley P, Hart GW*, et al.*, editors. Essentials of Glycobiology. Cold Spring Harbor (NY); 2015. p. 99-111.)

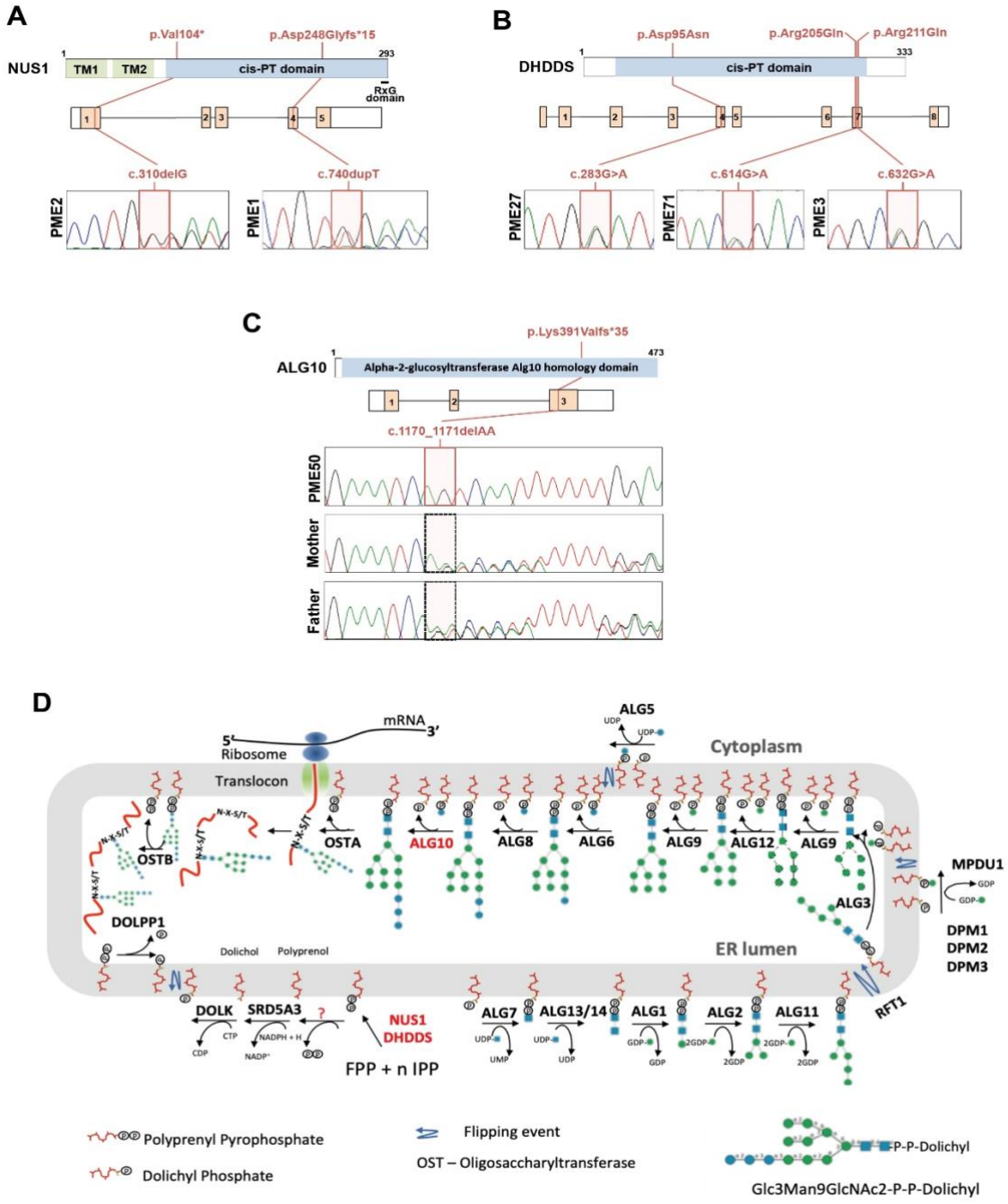

Abbreviations: *DHDDS* - Dehydrodolichyl Diphosphate Synthase Subunit; *FPP* - farnesyl pyrophospatase domain; *IPP* - isopentenyl pyrophosphatase domain; *NPC2* - Intracellular cholesterol transporter 2; *NUS1* - Nuclear Undecaprenyl Pyrophosphate Synthase 1 (Nogo-B Receptor), TM - transmembrane domain

Figure S3. **IGV snapshot of the two *SEMA6B* frameshift variants demonstrating low coverage.** For PME83 the c.1993delC variant was present in 3/6 reads. For PME25 the c.2032delG variant was present in 2/7 reads.

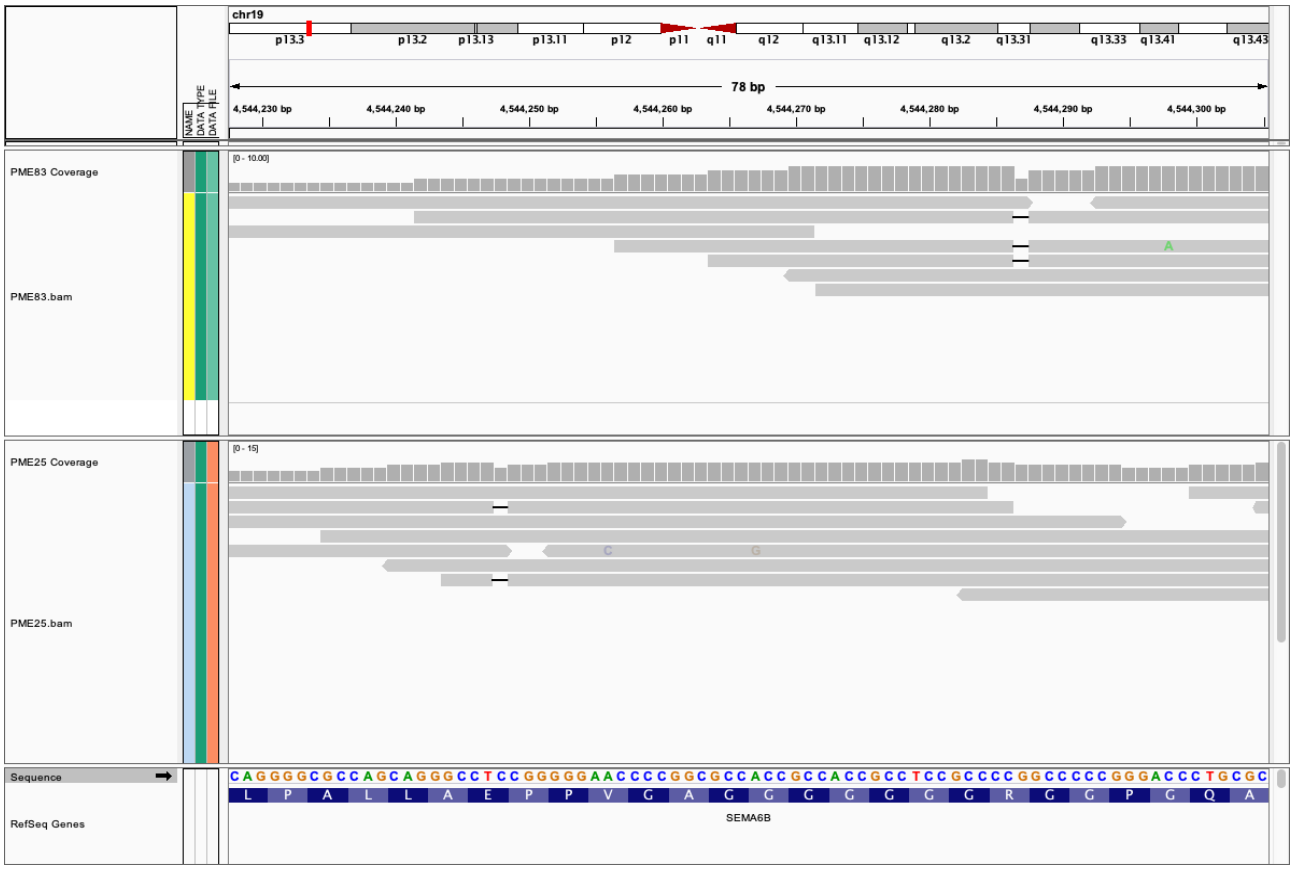

Figure S4: **Aberrant splicing caused by the deep intronic *CLN6* variant.** (**A**) Agarose gel electrophoresis showing the migration of RT-PCR products amplified from total RNA extracted from fibroblast cells of patient PME 15, using primers from exons 4 and 6 of *CLN6*. Two fragments are amplified from patient (P) cells. Controls (C) show a single strong amplicon. The size of the two fragments identified in the patient samples, based on sequence analysis, are shown on the right with the lower of the two corresponding to the expected 307-bp product. The fragments seen in controls also correspond to the expected product, based on sequence analysis, even though the fragments run differently from those in the patient samples. M indicates a 100-bp DNA ladder. (**B**) Sequence chromatogram of a control sample shows expected sequence in the exon 4-exon 5 boundary in the 307-bp amplicon. Sequence chromatogram from the 426-bp amplicon in the patient sample shows that the exon 4 sequence is followed by 119 bp of intronic sequence (shown only in part) before beginning of the exon 5 sequence. The position of the homozygous c.486+28T>C variant is indicated with an arrow. (**C**) Schematic representation of intron 4 of *CLN6* showing the position of the c.486+28T>C variant, the intronic ESE created by the variant and the non-canonical splice site (AG/GT) that is activated. The intronic sequence included in the 426-bp amplicon is shown in orange and the intronic sequence excluded from the mRNA is shown in green.

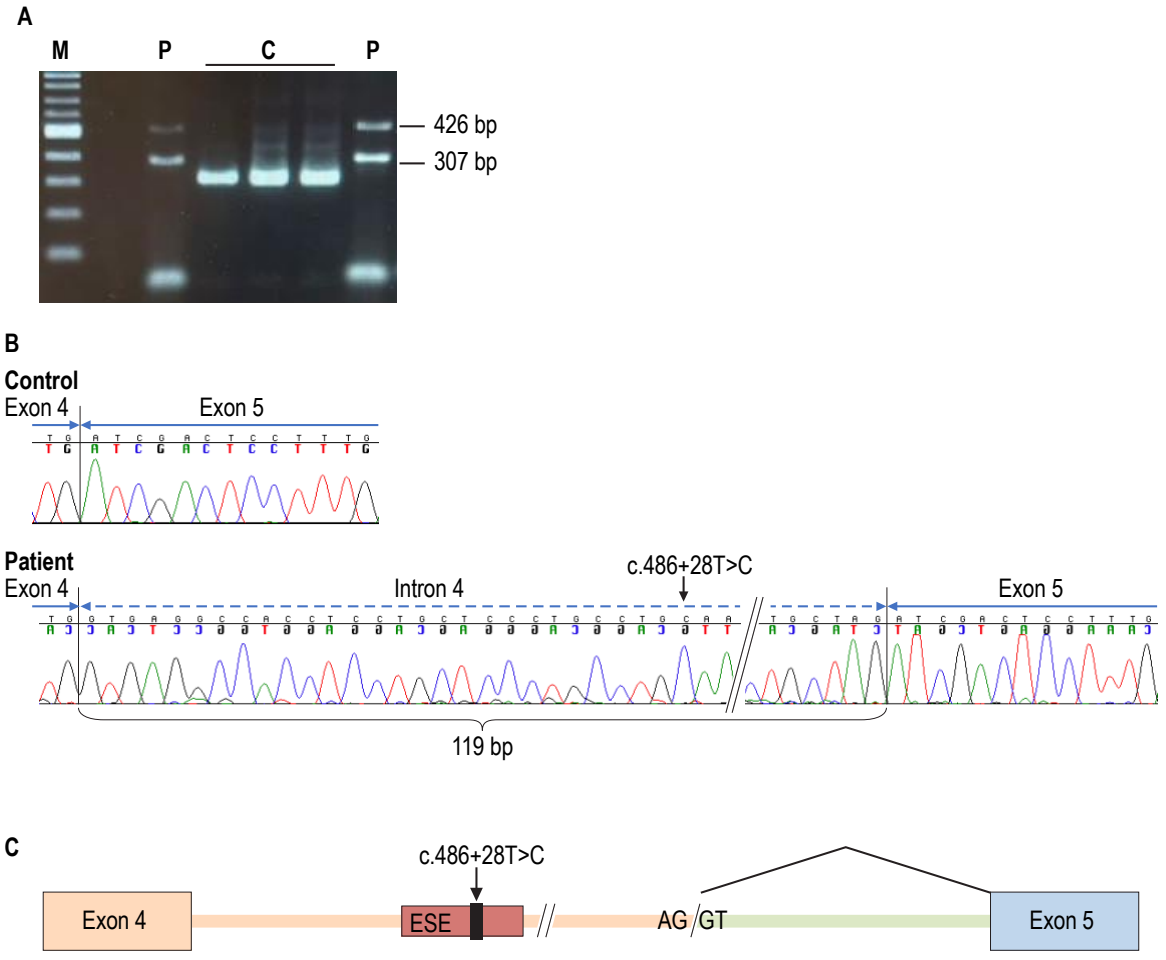

Figure S5. **Deletion confirmation of NEU1 was performed by quantitative PCR.** Primers for *NEU1* in exon 2 and exon 5 as well as adjacent non-deleted control gene C6orf48 were normalized to the single-copy gene β-microglobulin (B2M) using the ΔΔCt method in DNA from patient PME10, his affected brother and carrier father compared to controls. qPCR was performed using the IQ SybrGreen kit (Bio-Rad) on a CFX96 Touch qPCR system (Bio-Rad). Primer efficiencies and their linear range were determined by serially diluted genomic DNA and the presence of any unspecific amplification was excluded by melting curve analysis and agarose gel electrophoresis. All reactions were performed in triplicates.

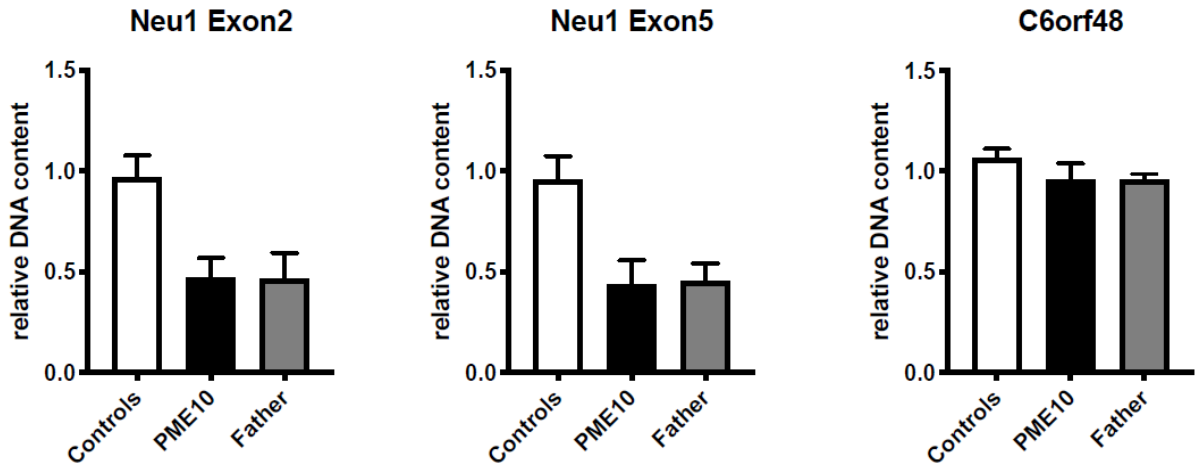

Figure S6. **Chr1q23.2 haplotype encompassing *PEX19* c.254C>T (p.A85V) variant.** Shared homozygous-by-descent haplotype (pink) found in the three patients of Maltese origin with *PEX19* variants. The haplotype length shared between the two unrelated families is much smaller (~1cM) consistent with a distant common ancestor.

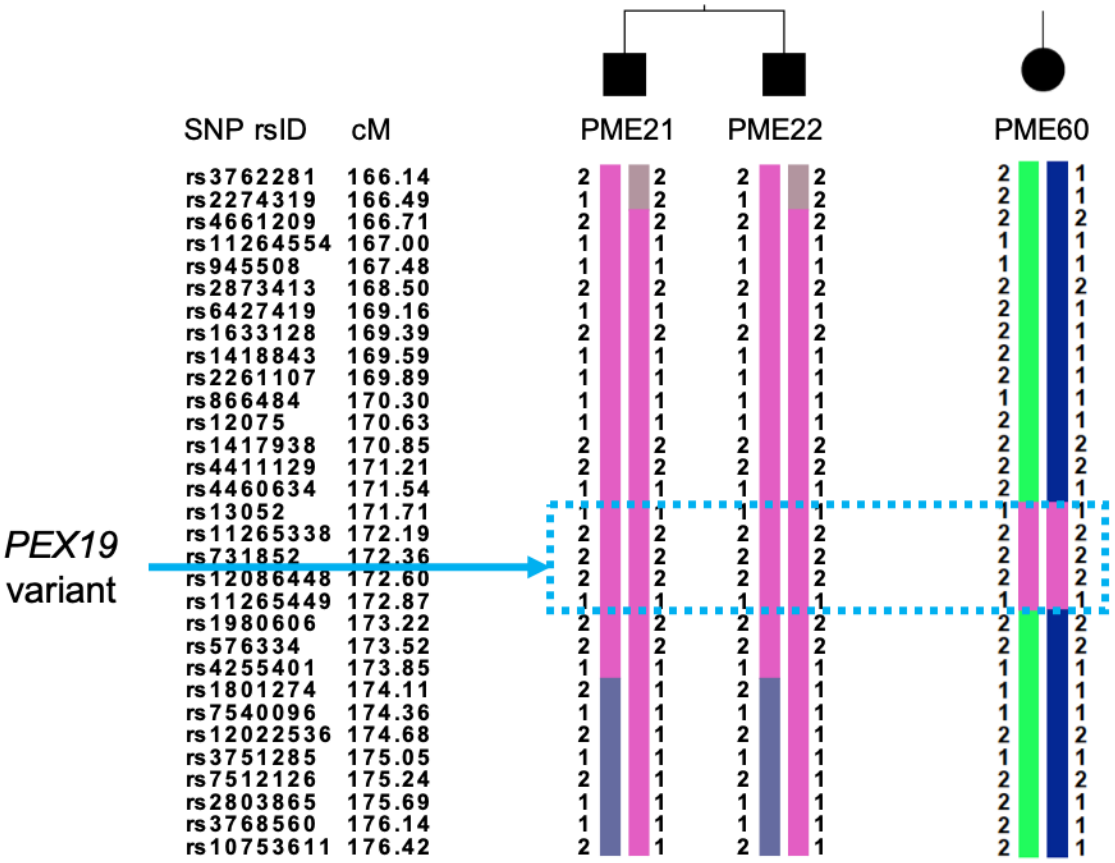

Figure S7: **Molecular modelling supports CACNA1A p.Asp1633Asn variant loss-of-function effect**. CACNA1A p.Asp1633 represents a conserved residue. The human sequence either side of Asp1633 is homologous with the rabbit Cav1.1 channel, enabling Pymol modelling of the structural impact of the p.Asp1633Asn variant identified in patient PME16. **(A)** Homology modelling of the human Cav2.1 Asp1633Asn mutation using the cryo-EM structure of the rabbit Cav1.1 channel Wu et al (2015) Science 350: aad2395-aad2395, and (2016) Nature 537: 191-196 - PDB accession number 3JBR **(B)** Amino acid sequence alignment of the of the human Cav2.1 channel (NCBI refseq NM_001127222.1; Protein ID = NP_001120694.1) and the rabbit Cav1.1 channel (protein ID = NP_001095190.1), using CLC sequence Viewer 7.7 (Qiagen, Aarhus, Denmark).

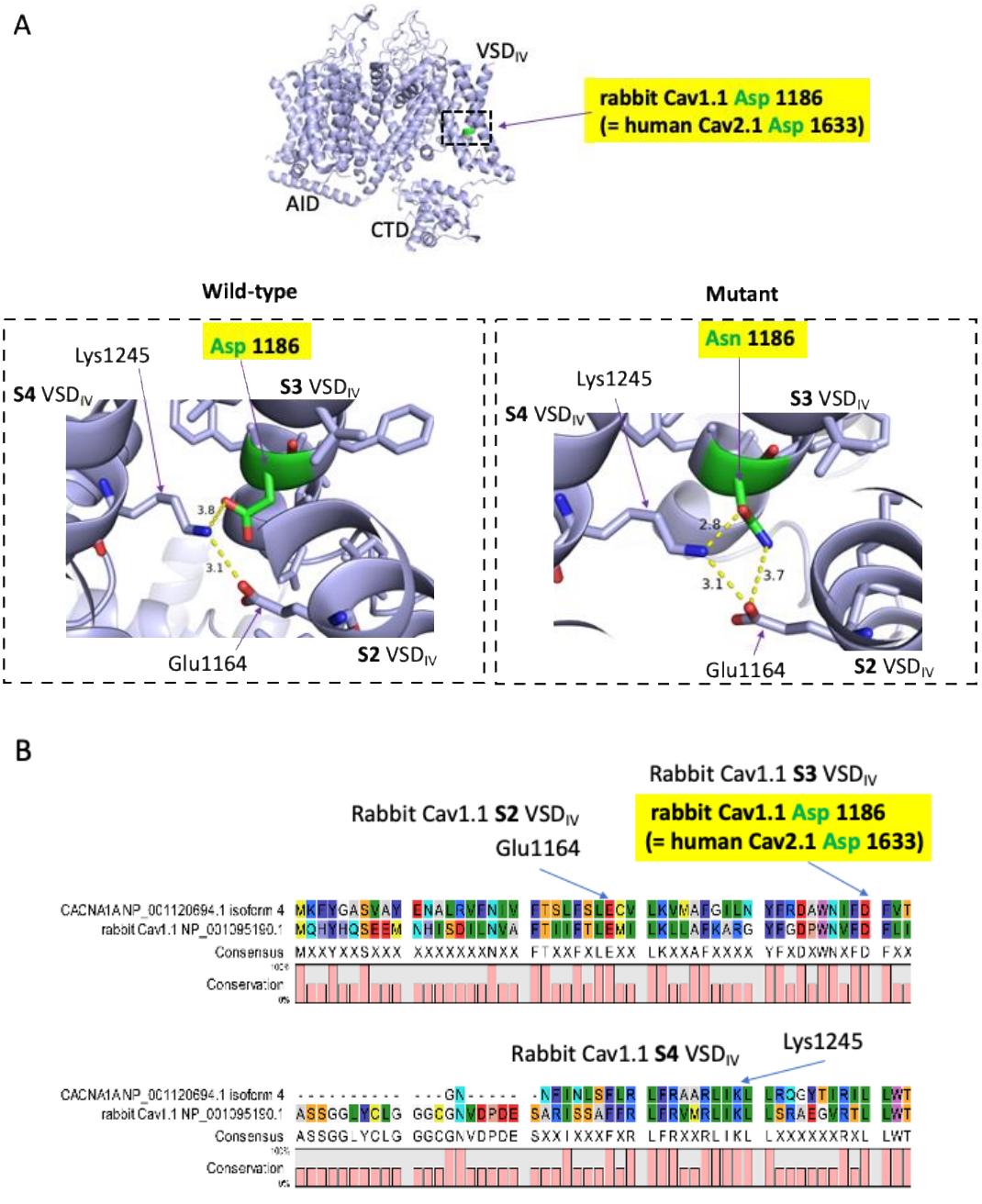

Symbols and abbreviations: Yellow dashed lines with number: distance between residues in Å; Red sticks: oxygen atoms; Blue sticks: nitrogen atoms; VSD: voltage sensor domain; CTD: C-terminal domain; AID: α1-interacting domain; S2, S3, S4: segments 2, 3, and 4. Residues involved in the interactions shown in panel (A) are marked by arrows in panel (B).

In the wild type channel, Asp 1633 is located in segment 2 of the voltage sensor domain IV (VSD_{IV}). In the human Cav2.1 channel, Asp 1633 corresponds to Asp 1186 of the rabbit Cav1.1 channel. Asp 1186 has a negatively charged sidechain, which interacts with the positively charged sidechain of Lysine 1245; Lys 1245 may also interact with the Glutamic acid (Glu) 1164; repulsion may occur between Asp 1186 and Glu1164.

In the mutant channel, the acidic Asp residue (with negatively charged sidechain) is replaced by the polar/neutral Asn 1186 residue. Asn 1186 may interact with both Lys 1245 and Glu 1164; whereas the polar interaction between Lys 1245 and Glu 1164 (that exists also in the wild-type channel) should remain unaffected. It's likely that the Asp1186Asn mutation (equivalent with Asp1633Asn) stabilises the interaction between the S4 and the S3 segments in VSD_{IV}. Because of the increased interaction between S3-S4, the mutation may compromise activation gating. As a result, the typical vertical (outward) movements of the S4 segment during activation may be impeded, leading to loss-of-function.

Consistent with the above structural modelling, a web-based machine learning model, capable of predicting loss-of-function (LoF) or gain-of-function effects in voltage gated calcium channels (Heyne HO *et al*. *Sci Transl Med*, 2020), predicted loss-of-function with a probability of 0.77, and pathogenicity with a probability of 0.87, for the p.Asp1633Asn variant.